

Electromechanical Sigma-Delta Modulators ($\Sigma\Delta$) Force Feedback Interfaces for Capacitive MEMS Inertial Sensors: A Review

Fang Chen, Xinxin Li, and Michael Kraft

Abstract—Analog-to-digital converters (ADC) based on sigma-delta modulators ($\Sigma\Delta$) are a popular choice for high resolution conversion from the analog to the digital domain. With relatively small modifications they also can be used as electromechanical $\Sigma\Delta$ (EM- $\Sigma\Delta$) force feedback interfaces for capacitive micro-electromechanical systems (MEMS) inertial sensors. Such interfaces are able to combine the benefits of force feedback and analog to digital conversion at relatively modest circuit cost. This paper provides a comprehensive review of EM- $\Sigma\Delta$ interfaces for capacitive MEMS inertial sensors. The principle and design methodology of EM- $\Sigma\Delta$ interfaces are introduced. A classification of EM- $\Sigma\Delta$ accelerometers and gyroscopes is presented, and a detailed analysis of different EM- $\Sigma\Delta$ architectures is given. The most representative EM- $\Sigma\Delta$ inertial sensors systems are discussed and compared with regard to their performance characteristics. In particular, the properties of various discrete and continuous-time techniques and a system parameter optimization methodology are illustrated through specific examples. Finally, current challenges and future development trends of EM- $\Sigma\Delta$ interfaces for inertial sensors have been identified.

Index Terms—MEMS, capacitive inertial sensors, EM- $\Sigma\Delta$, force feedback, discrete-time, continuous-time, optimized methodology

I. INTRODUCTION

Micro-electromechanical systems (MEMS) inertial sensors, comprising accelerometers and gyroscopes, are one of the most important types of silicon-based sensors [1]. Over the last decade, the field of inertial sensors has seen a significant increase in research effort and commercial products. Compared to traditional inertial sensors, MEMS devices have many

This work was supported in part by the National Natural Science Foundation of China (Grant no 61504159), Science and Technology Commission of Shanghai (Grant no 14521106100), Key Program of National Natural Science Foundation of China (Grant no 61234007).

F. Chen and X. Li are with the State Key Lab of Transducer Technology, Shanghai Institute of Microsystem and Information Technology, Chinese Academy of Sciences, Shanghai 200050, China (e-mail: fangchen@mail.sim.ac.cn; xxli@mail.sim.ac.cn). Corresponding author is Xinxin Li.

M. Kraft is with the Montefiore Institute, University of Liege, Wallonia, Liege 4000, Belgium. (m.kraft@ulg.ac.be)

advantages such as low cost, small size, low power consumption and their suitability for batch fabrication. Almost exclusively, MEMS inertial sensors are fabricated through some specialized micromachining processes (surface or bulk-micromachining, silicon-on-insulator, silicon-on-glass, etc.), and are combined with an interface circuit. The current market has been estimated to be worth over \$1000 million and keeps growing at a rate of 10-20% per year [2]. The growth in recent years has been achieved mainly by employing low-cost manufacturing technologies. As a result, the sensors are used increasingly in cost sensitive automotive and consumer applications, such as vehicle stability control, mobile phones, wearable electronics devices and many others [3-6]. However, emerging high-end applications are generating a growing demand for high performance MEMS inertial sensors with an increasing range of functionality including digital interfacing, self-testing, calibration and temperature compensation. This trend motivated the development of a variety of interface and control circuit systems.

In particular, MEMS inertial sensors using capacitive transduction have attracted considerable attention due to their advantages such as good thermal stability, high sensitivity and relatively simple batch-fabrication [1, 7-8]. Additionally, they are suitable for closed loop operation as electrostatic feedback can be used. A basic capacitive inertial sensor interface circuit is composed of a capacitance-to-voltage converter (C/V) followed by other signal conditioning circuitry, such as low-pass or band-pass filters and, optionally, an analog-to-digital converter (ADC). MEMS inertial sensors operating in an open-loop configuration (no feedback signal) result in a relatively simple and inherently stable sensor system suitable for low performance and cost sensitive applications. However, open-loop configurations cause the sensor performance to be sensitive to the parameters of the micromachined sensing element; for example, the sensitivity and bandwidth of the sensor are both related to the natural frequency of the mass-spring-damper system [9]. Moreover, the overall system linearity is affected by the linearity of each block in the sensor system chain. Also, the signal processing circuit, including the C/V and ADC, may need to satisfy challenging dynamic range (DR) requirements.

On the contrary, embedding the sensing element in a negative feedback closed-loop control system has many advantages, such as independence of the sensitivity-bandwidth tradeoff (to a large degree), better linearity, lower susceptibility to process and

temperature variations of the MEMS sensor and a higher and tunable dynamic range [9-12]. Furthermore, the C/V dynamic range and linearity specifications of the interface circuits can be relaxed compared to open-loop mode of operation. However, unlike macroscopic inertial mechanical sensor systems, for which the implementation of a feedback system is relatively simple, for a MEMS device the feedback design is challenging, due to the sensors dynamics, relatively high-frequency system dynamics and requirements for the close integration of the control system with the actual MEMS device. For capacitive accelerometers and gyroscopes the feedback signal typically is used to attain control over the proof mass position of the sensing element. The position is controlled by applying an electrostatic force feedback to the proof mass of the sensing element, which has to counterbalance the inertial force and simultaneously provides an accurate measurement of the input inertial force. Analog closed loop control systems are mainly based on a modified proportional-integral-derivative (PID) controller; however, this has some inherent disadvantages such as the inherently nonlinear feedback voltage to electrostatic force relationship [13, 14]. A linear electrostatic feedback force can only be generated under the assumption of small proof mass displacement (compared to the initial electrode gap). If the proof mass displacement becomes large, additionally the problem of electrostatic pull-in may occur leading to a non-recoverable condition and thus sensor failure [15].

An effective solution to overcome these disadvantages is to use a digital control strategy based on the principle of a sigma-delta modulator ($\Sigma\Delta$), which can preserve all advantages of closed-loop operation and concurrently produce a digital output in the format of a pulse density modulated bitstream [16, 17]. Sigma-delta modulation ($\Sigma\Delta$) is a technique normally used in high-resolution ADC. It combines sampling at rates well above the Nyquist rate with negative feedback and filtering in order to trade-off resolution in time with that in amplitude. In a $\Sigma\Delta$ ADC an analog loop filter is utilized to shape the quantization noise away from the signal band of interest. The inertial sensing element embedded in an electromechanical $\Sigma\Delta$ (EM- $\Sigma\Delta$) force feedback loop serves not only to detect the inertial input signal but also takes the role of the loop filter. The analog building blocks in the $\Sigma\Delta$ closed loop system include a C/V converter, a signal amplifier, a phase compensator and, optionally, some additional electronic filtering blocks. A single- or multi-bit quantizer converts the analog signal to an oversampled bit sequence, which is further processed digitally to produce the final sensor output signal. The digital output of the quantizer is converted back to the analog domain and is applied to the sensing element as a feedback signal in the form of an electrostatic force produced by the feedback voltage. Since the feedback voltage can only have discrete levels the feedback signal exhibits high linearity. At the same time, the $\Sigma\Delta$ provides implicit analog to digital conversion, eliminating the need for a stand-alone ADC. Thus, $\Sigma\Delta$ closed-loop interfaces represent an attractive architecture for high performance, digital MEMS inertial sensors.

This paper aims to provide a comprehensive review of research presented to date about EM- $\Sigma\Delta$ force feedback interfaces for capacitive inertial sensors. Following this

introductory section, Sec. II presents an overview of the principles of EM- $\Sigma\Delta$ force feedback techniques and makes a detailed analysis of different EM- $\Sigma\Delta$ architectures. Sec. III gives a general overview and classification of EM- $\Sigma\Delta$ accelerometers with respect to their implementation and performance characteristics. Sec. IV provides a comprehensive review on low and band-pass EM- $\Sigma\Delta$ gyroscopes. Optimization methodologies based on linearized and non-linear models for EM- $\Sigma\Delta$ gyroscopes and accelerometers are described in Sec. V, in which published EM- $\Sigma\Delta$ gyroscopes are also compared. Various issues and future prospects are discussed in Sec. VI, which is followed by conclusions in Sec. VII.

II. ELECTROMECHANICAL $\Sigma\Delta$ PRINCIPLES AND ARCHITECTURES

A. Principles

A $\Sigma\Delta$ is the combination of a delta (Δ) modulator and an additional integrator in the feed-forward path performing the summation; this architecture has been employed since Inose *et al.* [18] proposed it in 1962 as an ADC technique [19]. Fig. 1 shows the block diagram of a first order $\Sigma\Delta$; the difference between the input and the feedback signal is passed through a filter and digitized by a quantizer, with a resolution of one or several bits. The quantizer operates at a sampling rate significantly higher than twice the bandwidth of the input signal. The oversampled digital sequence contains the input signal and the noise from the quantization. Compared to a Nyquist sampling converter, a $\Sigma\Delta$ requires oversampling and shapes the quantization noise moving it to out-of-band frequencies.

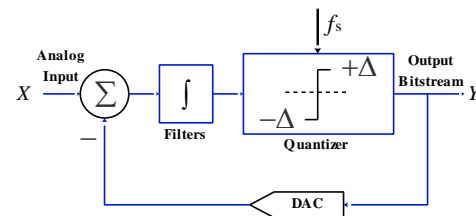


Fig. 1. Block diagram of a first order $\Sigma\Delta$

The capacitive inertial sensing element consists of a suspended, movable proof mass which is displaced by an inertial force. It thus can be modelled as a mass-damper-spring system of which the ratio of the force on the proof mass to its displacement in one direction can be approximated by a 2nd-order transfer function $M(s)$:

$$M(s) = \frac{1}{ms^2 + bs + k} \quad (1)$$

where m is the mass of proof mass, k is the effective spring stiffness, b is the damping factor. It can be regarded analogous to two cascaded electronic integrators commonly used in 2nd-order electronic $\Sigma\Delta$ ADC. The system level diagram of such a 2nd-order EM- $\Sigma\Delta$ loop is shown in Fig. 2, comprising a sensing element, an analog readout interface, a compensation network, a quantizer and a voltage to force converter in the feedback path. The EM- $\Sigma\Delta$ inertial sensor has a direct digital output signal in form of a pulse density modulated bit-stream, thus it can be directly interfaced to a digital signal processing

system. Assuming electrodes to either sides of the proof mass forming parallel plate capacitors, the digital feedback signal is converted to an electrostatic force F_{fb} acting on the proof mass, which can be expressed by the following equation [20]:

$$F_{fb} = \text{sgn}(D_{out}) \frac{\epsilon_0 A_{fb} V_{fb}^2}{2(d_0 \pm x)^2} \quad (2)$$

where ϵ_0 is the dielectric constant of vacuum, A_{fb} the area of the feedback electrode, V_{fb} the feedback voltage, d_0 the nominal gap between the proof mass and the electrodes to either side, x the deflection of proof mass from its rest position and D_{out} the momentary value of the digital quantizer output bit-stream, which is either a positive or negative reference feedback voltage ($\pm V_{ref}$). The electrostatic force can be regarded as approximately constant for small proof mass deflections ($x \ll d_0$). The quantizer introduces a quantization error, which can be modelled as an additional noise source [21]. It is desirable for a high signal-to-noise ratio (SNR) to have a quantization noise level of at least one order below both the mechanical (Brownian) noise and electronic noise levels [22]. Although the SNR of a 2nd-order EM- $\Sigma\Delta$ can be somewhat improved by increasing the sampling frequency, the SNR improvement has limitations due to the coupling between electronic and quantization noise in EM- $\Sigma\Delta$ [23, 24]. Furthermore, a higher sampling frequency leads to higher system power consumption. A better solution for increasing the SNR is to use a high-order EM- $\Sigma\Delta$ at lower sampling frequencies, which employ additional electronic filters and thereby achieving high-order quantization noise shaping in the signal band. As shown in Fig. 2, the mechanical noise and the input inertial force signal pass through the loop filter without attenuation within the signal band. The transfer function of the quantization noise ($QNTF$) is given by [25]

$$QNTF = \frac{1}{1 + M(s)K_{po}C_pH_sK_{fb}K_q} \quad (3)$$

where K_{po} is the gain of the capacitive readout circuit, C_p represents the transfer function of a compensator, H_s the transfer function of the additional electronic filters, and K_q the equivalent gain of the quantizer. According to equation (3), the 2nd-order mechanical loop filter (the sensing element) is cascaded with a compensator and additional electronic filters to obtain further quantization noise shaping. The implementation of a high-order EM- $\Sigma\Delta$ interface circuit can be either in the discrete-time (DT) or continuous-time (CT) domain. DT and CT interfaces have their own different characteristics; among others, CT interfaces can operate with a higher sampling frequency compared to DT interfaces. DT interfaces, on the other hand, are easy to map from a mathematical description into a practical circuit design [25]. A further challenge in the design of EM- $\Sigma\Delta$ is that there is no access to the internal nodes of the sensing element incorporated in the loop. As shown in Fig. 3, its main signal path comprises two integrators. The inner node is corresponding to the speed v of the proof mass and is not directly accessible. The inner node cannot be connected to subsequent electronic building blocks to form feed-forward or feed-back paths to or from the electronic integrators. Therefore, the overall structure misses one degree-of-freedom to have full control of the loop roots. The design methodology of high-order

EM- $\Sigma\Delta$ interface is thus different from conventional $\Sigma\Delta$ ADC.

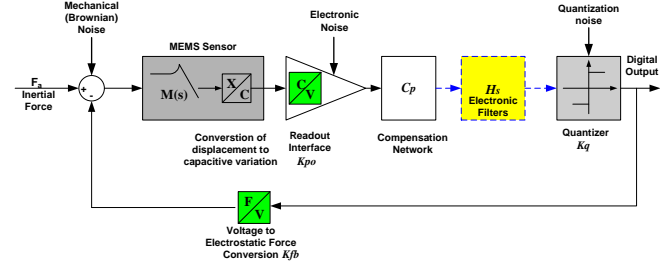


Fig. 2. Typical 2nd and high-order EM- $\Sigma\Delta$ interface system for a MEMS inertial sensor [12].

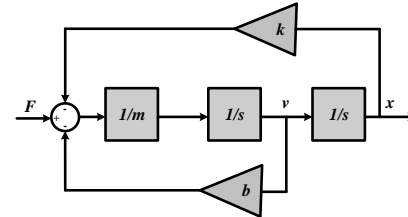


Fig. 3. System level diagram of the mechanical sensing element, which can be modelled as a 2nd-order mass-damper-spring system.

B. Stability

An electro-mechanical $\Sigma\Delta$ is an unstable system without compensation because of the 180 degree phase shift originating from the sensing element for frequencies above the resonance. Smith *et al.* [26] used an over-damped sensing element to move the two mechanical poles to the real axis at a high and low frequency, respectively. By operating the feedback loop below the high-frequency pole, effectively only first-order filtering was realized. Using a lead compensator requires additional circuitry but avoids the aforementioned problems. A compensator such as a first-order FIR filter ($T(z) = \alpha z^{-1}$) can add a left half-plane zero to the loop transfer function to decrease the phase shift at unity-gain frequency, while principally retaining the 2nd-order noise shaping characteristic of the sensing element [20]. Dong *et al.* [25] proposed a systematic method to design high-order EM- $\Sigma\Delta$ based on a linearized system model, followed by extensive system level simulations to determine the optimal zero of the compensator. Raman *et al.* [27] suggested an unconstrained architecture, so that the inner node of the mechanical sensing element is not required. As can be seen from Fig. 4, this method starts with an unconstrained, purely electrical Nth order $\Sigma\Delta$ architecture, as shown in Fig. 4(a). By using block diagram reconstruction, the feedback path of the inner node (after the first integrator) is converted to a feedforward path, as shown in Fig. 4(b). The feedforward path can be shifted so that the structure shown in Fig. 4(c) is obtained; this is not only still equivalent to the one shown in Fig. 4(b) but also eliminates the need for the feedback path to the inaccessible inner node. Thus, the first two electrical integrators can be replaced with two mechanical integrators. The resulting structure retains the same order as the original purely electrical $\Sigma\Delta$, and does not need a compensator for loop stability.

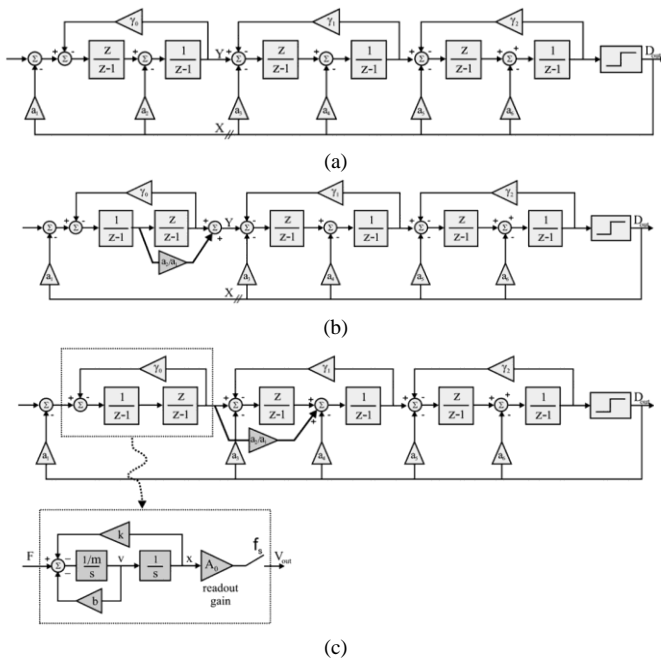


Fig. 4. Converting a purely electrical $\Sigma\Delta M$ to an unconstrained EM- $\Sigma\Delta M$. (a) An unconstrained electrical $\Sigma\Delta M$ structure [25]. (b) The feedback path to the inner node of the first resonator stage can be converted to a feedforward path. (c) The feedforward path can be shifted and replaced by the micromechanical sensor. From [27].

However, the unconstrained $\Sigma\Delta M$ architecture and conventional lead compensation results in stability margins that are inadequate for high- Q (vacuum packaged) sensing elements. This problem is due to high-order resonance modes of the sensing element arising from the electrostatic comb fingers, which normally are sufficiently damped at atmospheric pressure, but become highly underdamped in vacuum resulting in a phase lag approaching -360° . Ezekwe *et al.* [28, 29] used a different compensator that utilizes positive feedback to introduce a phase lead of 180° at all frequencies, which is sufficient to compensate the phase lag introduced by the parasitic modes. The block diagram of the EM- $\Sigma\Delta M$ feedback loop with positive feedback compensator is shown in Fig. 5. Furthermore, other factors including the time delay between the position sense and feedback pulse, the sampling frequency f_s and whether sensing and feedback use separate or common electrodes influence the stability and performance of the EM- $\Sigma\Delta M$ loop. This necessitates a tradeoff between these design choices.

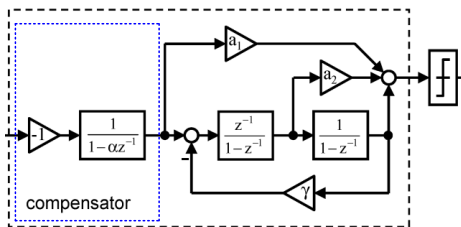


Fig. 5. Positive feedback compensator in a EM- $\Sigma\Delta M$ interface described in [28, 29].

C. Single loop architectures

Several loop structures have been described for implementing a single-loop high-order EM- $\Sigma\Delta M$; they are trade-offs between structure complexity and the freedom of choosing the shape of the signal-transfer-function (STF) and the

position of the noise-transfer-function (NTF) zeros [30]. The most commonly used structure is the cascaded integrator with distributed feedback (CIDF) architecture, as depicted in Fig. 6. It contains a cascade of several delaying integrators with feedback signals that are scaled by coefficients a_i ($i = 1, 2, \dots$) and fed to each integrator. The distributed feedback architecture bypasses the mechanical sensing element and therefore contributes compensating zeros, whose values depend on the feedback coefficients as well as the parameters of the sensing element. Furthermore, the feedback voltage of this topology cannot be adjusted without tuning the values of the coefficients a_i [30]. Dong *et al.* [25] analysed the total in-band noise of a typical CIDF architecture, which is mainly determined by the quantization noise at the upper end of the signal band. It thus limits the maximum obtainable signal bandwidth and it is desirable to further reduce the total in-band quantization noise power.

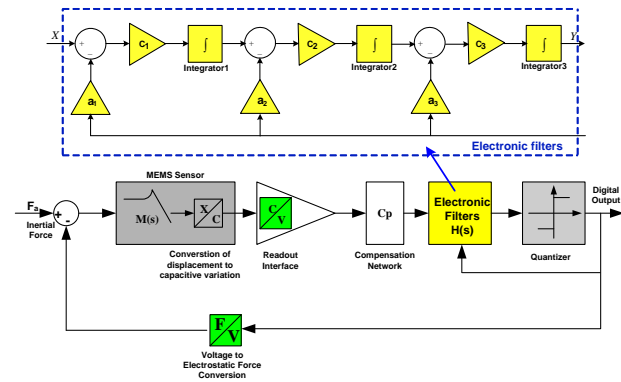
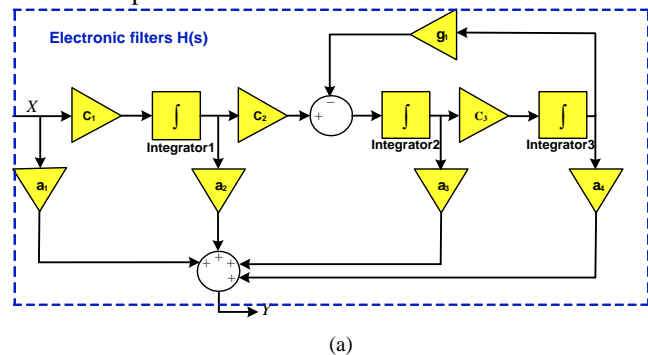


Fig. 6. Cascaded integrators with distributed feedback architecture for a EM- $\Sigma\Delta M$ [25].

A single loop high-order EM- $\Sigma\Delta M$ can be constructed by using several local feedback paths in the loop filter to shape the quantization noise at the end of the signal band [31]. Fig. 7 (a) and (b) show the architecture of an electronic filter with feed-forward with local resonators (FFLR) [32-33], and distributed feedback loops with local resonators (DFLR) [34], respectively. The local feedback path g_i ($i = 1, 2, \dots$) will create a local resonator, which produces notches to cause fast decay of the signal magnitude in the stop-band and thus further suppresses the quantization noise. The architecture in Fig. 7(a) does not contain signal paths bypassing the sensing element since it is in series with the filter and the quantizer. The feedback range is easily adjusted by varying the magnitude of the feedback pulses.



(a)

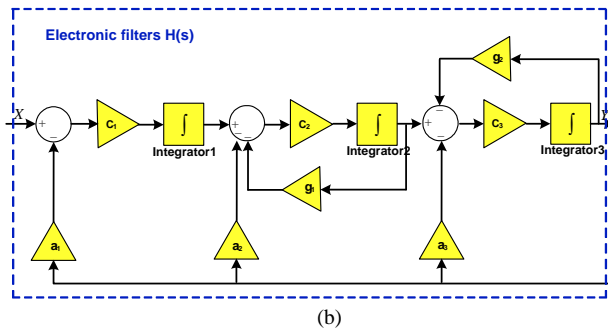


Fig. 7. The electronic filter, $H(s)$, for (a) feed-forward loops with local resonators and (b) distributed feedback loops with local resonators architectures. From [32-34].

Normally, a single loop architecture has a low susceptibility to analog component mismatch [35]. In addition, the quantization noise is randomized by the high-order loop; therefore, limit cycle tones are less likely to occur [25].

D. Cascaded multi-stage architectures

In multi-stage architectures, an EM- $\Sigma\Delta$ force feedback loop and several lower order purely electronic $\Sigma\Delta$ are cascaded to construct multi-stage noise shaping (MASH) architectures, such as MASH2- j , MASH2- $j-k$ ($j, k = 1, 2, \dots$). Fig. 8 shows a system level view of a MASH2-2 EM- $\Sigma\Delta$ [35]. It consists of a 2nd-order EM- $\Sigma\Delta$ and a purely electronic 2nd-order CDF $\Sigma\Delta$. In the ideal case, the quantization noise, $Nq1$, from the 2nd-order EM- $\Sigma\Delta$ is scaled by the interface gains (K_1 and K_2), digitized by the purely electronic $\Sigma\Delta$ and then cancelled by the digital filters D1 and D2. Ideally, the only noise that appears in the overall modulator output is the quantization noise, $Nq2$, of the electronic $\Sigma\Delta$, which will be shaped by an order equal to the sum of all stage orders. An advantage of MASH architectures is that the quantization noise signals for all of the stages other than the first one are very similar to true white noise [35].

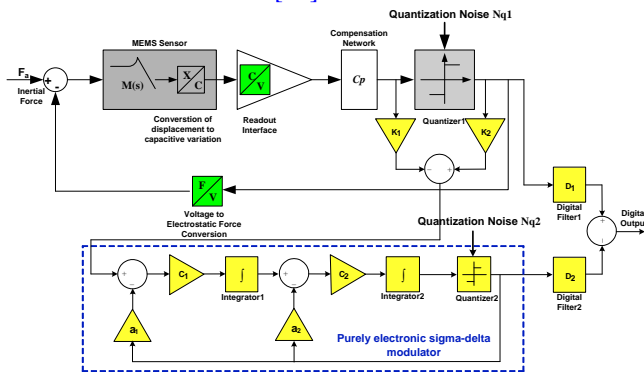


Fig. 8. An EM- $\Sigma\Delta$ force feedback loop based on MASH2-2 architecture [35].

MASH architectures have excellent stability properties and a high overload input threshold for low-order stages. They also have the advantage of a high dynamic range and high order noise shaping performance, comparable to a high order $\Sigma\Delta$ single loop architecture [36]. The drawback of MASH architectures is the need for precise filter coefficient matching between the digital filters and the analog components of the modulators. This means that the parameters of the sensing

element need to be known accurately; however, they are subject to fabrication tolerances. Any mismatch will lead to quantization error leakage from the first stage, which will substantially degrade the overall performance of the modulator [37]. This is the main reason why MASH architectures have to date not been used more extensively.

III. ELECTROMECHANICAL $\Sigma\Delta$ ACCELEROMETER

A. 2nd-order $\Sigma\Delta$ accelerometers

Henrion *et al.* [38] first proposed a 2nd-order EM- $\Sigma\Delta$ for a capacitive MEMS accelerometer in 1990. As in the above discussion, the accelerometer was considered as two cascaded integrators, thus forming a 2nd-order EM- $\Sigma\Delta$ control loop. Together with the electronic position sense circuit and quantizer, it formed an oversampled ADC in which the accelerometer provided 2nd-order noise shaping for frequencies above its resonance. The accelerometer sensing element consisted of a 500 μ m thick single-crystalline-silicon (SCS) spring-mass layer sandwiched between two identical single crystalline silicon layers. The displacement of the proof mass was sensed and controlled by pairs of concentric hexagonal-shape force and sense electrodes, located at the top and bottom of the mass. Identical patterns of the force and sense electrodes were located on the top and bottom covers, opposite their corresponding force and sense electrodes on the proof mass surfaces. The measured noise floor was below 10 μ g/ $\sqrt{\text{Hz}}$ and the dynamic range (DR) was approaching 120dB. From 1992, Berkeley Sensor & Actuator Center (BSAC), US did extensive research on 2nd-order EM- $\Sigma\Delta$ for capacitive accelerometers [39-42]. Yun and Howe *et al.* [39] presented a surface micromachined accelerometer with digital electronic feedback using a second-order $\Sigma\Delta$ technique. This accelerometer included a self-testing mode to ensure its functionality. Boser *et al.* [40, 41] presented a monolithically fabricated 2nd-order $\Sigma\Delta$ micromachined accelerometer based on polysilicon surface micromachining and CMOS integrated circuits, which achieved a full-scale (FS) range of $\pm 5g$, a DR of 50dB in a bandwidth of 50Hz and a resolution of 1.6mg/ $\sqrt{\text{Hz}}$ with a sampling frequency f_s of 500kHz. In 1999, Lemkin *et al.* [42] reported an integrated three-axis surface micromachined accelerometer with a CMOS position-sense interface and digital offset-trim electronics. By enclosing the proof mass in a one-bit $\Sigma\Delta$ feedback loop, one-bit forcing was achieved by applying a feedback voltage V_{fb} across one sense capacitor while applying zero potential difference across the second sense capacitor during the feedback phase; this is illustrated in Fig. 9. The measured DR within 100Hz was 84dB, 81dB, and 70dB and the noise floor 110 μ g/ $\sqrt{\text{Hz}}$, 160 μ g/ $\sqrt{\text{Hz}}$, and 990 μ g/ $\sqrt{\text{Hz}}$ along the x-, y-, and z-axes, respectively. A FS range of $\pm 18g$ was achieved by increasing the feedback pulse to 3V.

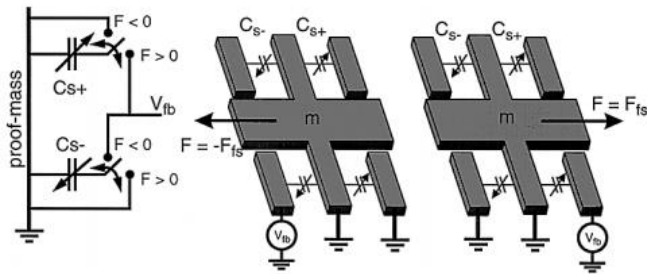


Fig. 9. One-bit force-feedback principle of a single axes $\Sigma\Delta M$ feedback loop used by Lemkin *et al* [42].

A detailed noise analysis of 2nd-order EM- $\Sigma\Delta M$ capacitive accelerometers with the goal of achieving sub- μg resolution was presented by Najafi *et al.* [43, 44]. The block diagram of the implemented CMOS circuit is shown in Fig. 10, which could operate the sensing element in open-loop or $\Sigma\Delta M$ force-rebalance modes. The circuit consisted of a switched-capacitor charge integrator, digital feedback (latching comparator and digital compensator), a clock generator, and a start-up circuit. The Brownian noise, front-end amplifier thermal noise, kT/C noise, mass residual motion, sensor charge referencing voltage (SCRV) noise, and quantization noise were considered and identified as the main noise components affecting the $\Sigma\Delta M$ accelerometer performance. The noise analysis and the test results showed that in $\Sigma\Delta M$ closed-loop mode of operation, the mass residual motion becomes critical especially at low sampling frequencies, whereas the amplifier and SCRv noise sources become dominant at high sampling frequencies. The accelerometer had $0.7\mu\text{g}/\sqrt{\text{Hz}}$ Brownian noise and approximately 1kHz bandwidth. The expected noise floor in the 2nd-order EM- $\Sigma\Delta M$ closed loop operation was around $1.5\mu\text{g}/\sqrt{\text{Hz}}$ using a sampling frequency, f_s higher than 1MHz.

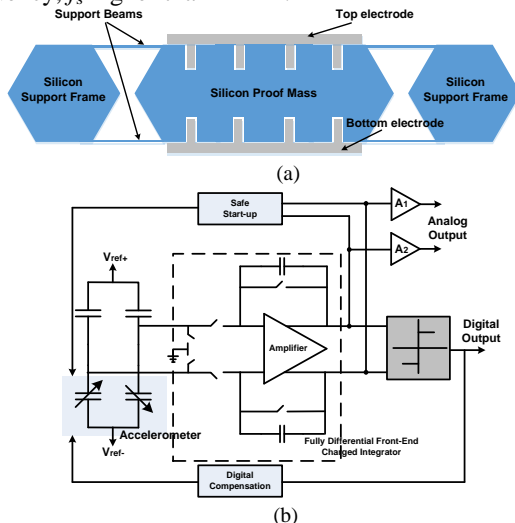


Fig. 10. (a) Accelerometer sensing element and the major blocks of the interface circuit (b) presented by Najafi *et al.* From [43, 44].

B. Single loop high-order $\Sigma\Delta M$ accelerometer

The first 3rd-order EM- $\Sigma\Delta M$ accelerometer with single bit quantization was presented by Smith *et al.* [26]; the system diagram is shown in Fig. 11. Previously discussed 2nd-order EM- $\Sigma\Delta M$ accelerometers have relatively poor noise shaping at low frequencies since the low frequency gain of the integrators

implemented by the sensing element is limited by the inverse of the effective spring constant of the proof mass suspension system [25]. The proposed 3rd-order EM- $\Sigma\Delta M$ accelerometer increased the SNR by an additional integrator in the loop. The accelerometer sensing element comprised a movable proof mass suspended by flexible cantilevers between two fixed electrodes. During the force feedback phase, the sensing element was disconnected from the readout circuit and the proof mass actuated towards the center position. However, the overall EM- $\Sigma\Delta M$ only provided 2nd-order noise shaping. As the second pole of the accelerometer (poles at 5Hz and 13kHz) was much higher than the signal bandwidth, it did not influence the noise shaping in the signal band. The two-chip sensor system had a noise floor of $10\mu\text{g}/\sqrt{\text{Hz}}$ at a sampling frequency f_s of 80kHz in a 5Hz bandwidth.

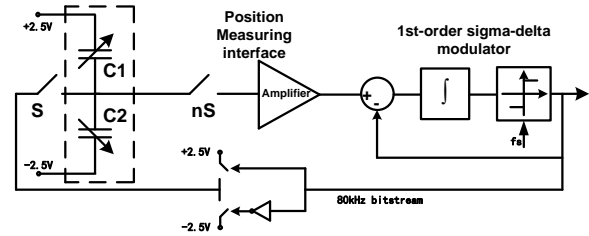


Fig. 11. A third-order $\Sigma\Delta M$ accelerometer proposed by Smith *et al* [26].

Wu *et al.* [45] first developed a 3rd-order EM- $\Sigma\Delta M$ accelerometer with 3-bit quantization. The simulation results showed that for a 1MHz sampling frequency, a SNR of 76dB could theoretically be achieved within a 2kHz signal bandwidth. However, only the pickoff preamplifier was experimentally verified. Kajita *et al.* [46] demonstrated another 3rd-order noise-shaping accelerometer, also enhancing the SNR by the addition of an electronic integrator in the loop. In 2005, Petkov *et al.* [23-24] presented a 4th-order switched-capacitor EM- $\Sigma\Delta M$ with feed-forward summation architecture for a lateral accelerometer with 6kHz resonant frequency, resulting in a resolution of $150\mu\text{g}/\sqrt{\text{Hz}}$ using a sampling frequency f_s of 850kHz. The interface chip was fabricated in a standard $0.5\mu\text{m}$ CMOS process. Fig. 12 shows a block diagram for the 4th-order $\Sigma\Delta M$, which did not contain signal paths bypassing the sensing element. The locations of the compensating zeros were well controlled and stable over temperature. Since the sensor appeared in series with the filter and the quantizer, the feedback range could easily be adjusted by varying the magnitude of the feedback pulses. It was designed as a closed loop interface for both gyroscopes and accelerometers. By simply assigning the feedback gain coefficient $\gamma=0$, the architecture can operate as a fourth order low-pass $\Sigma\Delta M$ interface for accelerometers.

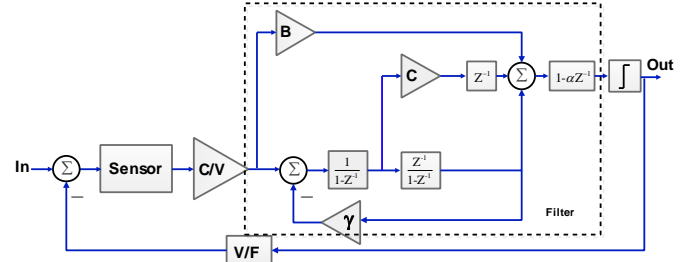


Fig. 12. 4th-order EM- $\Sigma\Delta M$ interface with feed-forward architecture proposed by Petkov *et al* [23].

Amini and Ayazi *et al.* [47-48] implemented a 3V switched-capacitor 4th-order CIDF $\Sigma\Delta$ CMOS interface circuit for closed-loop operation of a lateral capacitive micro-gravity SOI accelerometer. As shown in Fig. 13(a), accelerometers were fabricated using 120 μ m thick SOI substrates with an added solid mass resulting in a proof mass size of 3 \times 5mm². Fig. 13(b) illustrates the overall block diagram of the implemented 4th-order closed-loop EM- $\Sigma\Delta$ accelerometer system. The front-end read-out circuit comprised a switched-capacitor charge amplifier followed by two cascaded switched-capacitor integrators with distribute feedback and a two-level quantizer and feedback network. The closed-loop system was inherently stable as the accelerometer was over-damped (low- Q). The measured resolution was 4 μ g/ \sqrt Hz and the output DR of 95dB (20Hz) with an OSR of 40 (sampling frequency was 40kHz). The bias instability was 2~8 μ g for 12 hours.

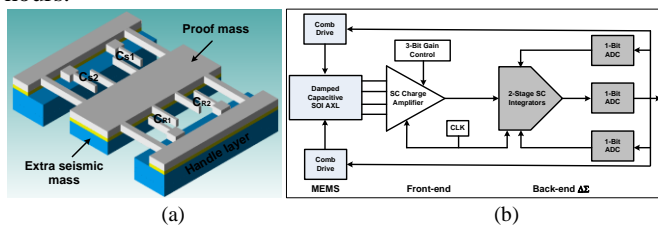


Fig. 13. (a) Schematic diagram of an SOI accelerometer with added seismic mass (b) Overall block diagram of the 4th-order fully differential switched-capacitor EM- $\Sigma\Delta$ interface. From [47].

Dong and Kraft *et al.* [49] implemented a 5th-order CIDF EM- $\Sigma\Delta$ interface circuit with an in-plane SOI accelerometer sensing element with a large proof mass (4 \times 7mm²) [50] by using CT off-the-shelf electronic components on a PCB (printed circuit board); the system level diagram is illustrated in Fig. 14(a). The experimental results indicated a noise floor of 0.1mg/ \sqrt Hz. The performance of this accelerometer was mainly degraded by the electronic noise injected by the electronic circuit and harmonic distortion. Compared with a 2nd-order EM- $\Sigma\Delta$, the sensing element cascaded with three electronic integrators led to better signal to quantization noise ratio, as illustrated in Fig. 14(b). An improvement was reported in 2006; Dong *et al.* [51] analysed the nonlinearity of the applied electrostatic force with respect to the mass position during the feedback operation. The Taylor expansion of equation (2) can be derived as:

$$F_{fb} = \frac{\epsilon_0 A_{fb} V_{fb}^2}{2d_0} [1 - \text{sgn}(D_{out}) 2(\frac{x}{d_0})^1 + 3(\frac{x}{d_0})^2 \dots] \quad (4)$$

Equation (4) indicates that the feedback force has harmonic content which will lead to a reduction in the SNR. It became evident that the small but non-zero residual proof mass motion modulated the feedback electrostatic force and degraded the SNR. An effective linearization scheme was proposed to alleviate this effect. The circuit was implemented on a PCB and a measured noise floor of 32 μ g/ \sqrt Hz (-110dB) was achieved. Chen *et al.* [52] proposed a 6th-order CT EM- $\Sigma\Delta$ interface for a vacuum accelerometer based on a DFLR $\Sigma\Delta$ architecture. The measured noise floor achieved was 15 μ g/ \sqrt Hz within a 500Hz bandwidth. Its noise performance, however, did not further improve compared to a 5th-order interface, due to the accumulated electronic noise from the cascaded four CT

integrators. Furthermore, the complexity of the interface increased due to the required analog filters.

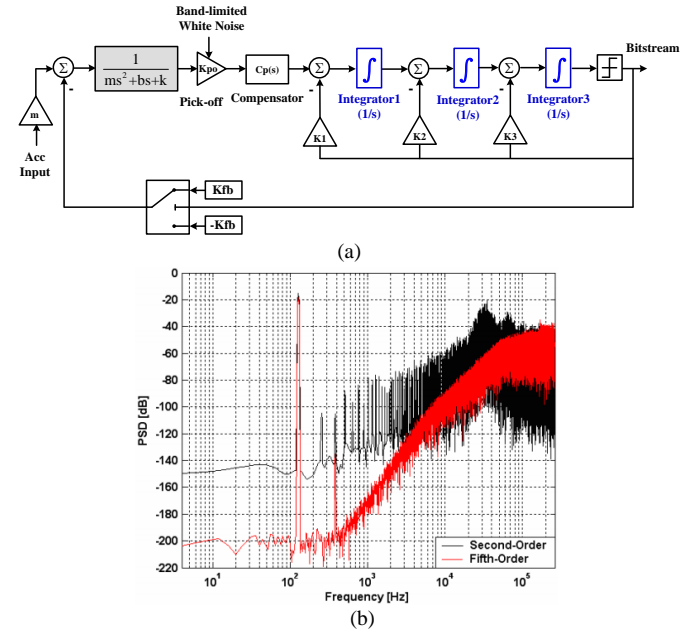


Fig. 14. (a) A 5th-order EM- $\Sigma\Delta$ interface proposed by Dong *et al.*[49] (b) Noise shaping comparison between 2nd and 5th-order EM- $\Sigma\Delta$ interface [25].

Even though aforementioned EM- $\Sigma\Delta$ accelerometers [23, 47, 52] achieved low noise, μ g resolution and large dynamic range, the sensing elements generally have a relatively large proof mass, and their FS range is limited. Sonmez and Akin *et al.* [53] designed and implemented a 4th-order switched capacitor EM- $\Sigma\Delta$ interface circuit in a standard 0.35 μ m CMOS process, which could be used in a feed-forward architecture [23] and an unconstrained architecture [27]. The system level diagram is shown in Fig. 15. The stability could be adjusted by electronic feed-forward and feedback paths. The coefficients (A-E) were configurable for a variety of accelerometer sensing elements. The employed sensing element had a structural thickness of 35 μ m and a proof mass of 264 μ g packaged at ambient pressure. In the feedback phase, the front-end C/V was disconnected from the electrodes and a high voltage (6-14V) pulse was applied to the sensor. The system achieved up to a \pm 40g FS range with a feedback voltage of 9.3V, 131.9dB DR at 1Hz, a minimum noise floor of 6 μ g/ \sqrt Hz, and a bias instability of 6.4 μ g.

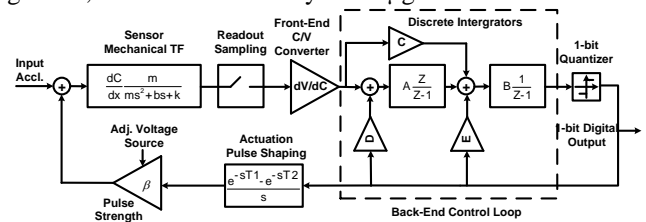


Fig. 15. Block diagram of the 4th-order unconstrained EM- $\Sigma\Delta$ accelerometer. From [53]

Dual quantization techniques can be another promising approach to the design and implementation of an EM- $\Sigma\Delta$ interface [54, 55]. As shown in Fig. 16(a), the control system comprised an analog and digital part. In the analog part, the proof mass displacement of the sensing element was measured and subsequently digitized using a multi-bit ADC.

The multi-bit digital output was then fed to the digital part to provide high-order quantization noise filtering. The output of the digital part was generated by a single bit digital quantizer. The cascaded electronic filters part was implemented using a field programmable gate array (FPGA). The FPGA offers the designer extra flexibility to tailor and optimize high order EM- $\Sigma\Delta$ architectures. Pastre *et al.* [54, 55] presented a MEMS-based 5th-order EM- $\Sigma\Delta$ capacitive accelerometer implemented with this approach. The $\Sigma\Delta$ loop was implemented as mixed signal circuit, as shown in Fig. 16(b). The 5th-order loop filter had a 2nd-order analog and a 3rd-order digital part. The complete mixed-signal front end was integrated in a 0.6 μ m CMOS process. An external reconfigurable 3rd-order digital filter was implemented in an FPGA to increase the total loop order and thus improve the system resolution. The system had a FS rang of 11g, a bandwidth of 300Hz and a noise floor of 1.15 μ g/ $\sqrt{\text{Hz}}$, corresponding to a DR of 19bits (119dB) over the 300Hz bandwidth.

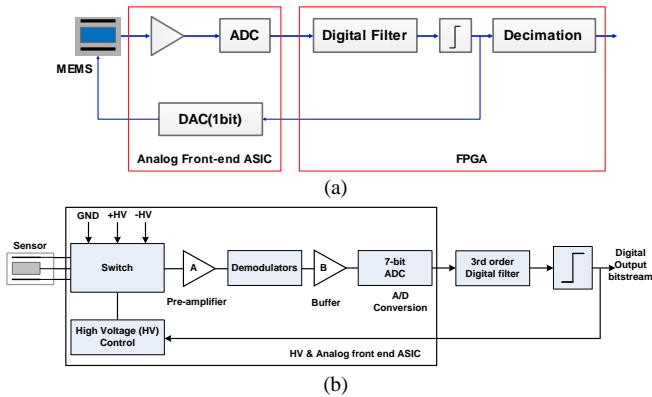


Fig. 16. (a) Block diagram of dual quantization EM- $\Sigma\Delta$ force feedback loop (b) 5th-order dual quantization EM- $\Sigma\Delta$ accelerometer proposed by Pastre *et al.* From [54, 55].

Zwahlen and Dong *et al.* [56-59] further developed a one-bit 5th-order EM- $\Sigma\Delta$ capacitive accelerometer architecture, targeting inertial navigation applications; the system diagram is shown in Fig. 17(a) and a PCB prototype in Fig. 17(b). The accelerometer sensing element was a bulk micromachined capacitive sensor with 11g input FS range over a 300Hz bandwidth. Measurements indicated a long-term bias stability of ± 0.1 mg (24hours), an in-band noise floor of 1 μ g/ $\sqrt{\text{Hz}}$ and a DR of 22.2bits in a 1Hz bandwidth or 18.1bits in a 300Hz bandwidth. The performance is comparable to standard inertial navigation accelerometers such as the Honeywell Q-Flex^R 2000-030 [60], which is the predominant sensor used in commercial and military aircraft inertial navigation systems. The results demonstrated that high-order EM- $\Sigma\Delta$ MEMS accelerometers can match the performance of expensive quartz macroscopic electro-mechanical sensors. Bringing MEMS accelerometers towards inertial navigation grade level, significant design effort on bias stability was required. In 2012, Zwahlen *et al.* [57] took advantage of the high mechanical stability of the MEMS accelerometer and reported significant progress on bias stability and temperature sensitivity through system optimization. For a FS range of 15g and a shock survivability up to 4000g the reported performance characteristics were 10 μ g bias stability during warm-up, a bias temperature slope below 200 μ g/ $^{\circ}\text{C}$, a scale factor temperature

slope below 100ppm/ $^{\circ}\text{C}$ and a white noise floor below 2 μ g/ $\sqrt{\text{Hz}}$. With these performance metrics EM- $\Sigma\Delta$ capacitive accelerometers are now competing with traditional high performance macroscopic electro-mechanical accelerometers on the market.

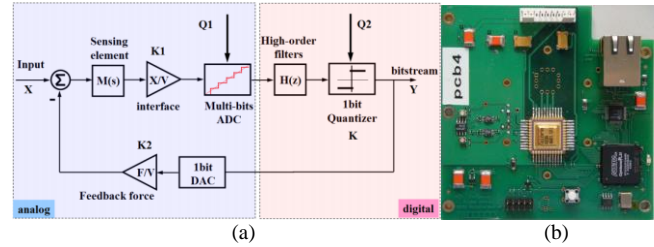


Fig. 17. (a) System block diagram and (b) PCB prototype of dual quantization mixed-signal EM- $\Sigma\Delta$ accelerometer proposed by Zwahlen and Dong *et al.* From [56-58].

Most of the previously reported EM- $\Sigma\Delta$ accelerometers used low- Q mechanical elements, 4th or 5th order architectures and a single-bit quantizer. High oversampling ratios, high-order noise shaping or multi-bit quantizer feedback are effective methods to improve the noise shaping for a single loop EM- $\Sigma\Delta$ accelerometer. However, they all have limitations: increasing the sampling frequency may lead to interactions among different noise sources and increase power consumption [20]. Realizing a multi-bit DAC for an electrostatic feedback force with high linearity is challenging because electrostatic actuation is inherently nonlinear. Although the linearity of the feedback signal can be improved by using linearization schemes [51], the feedback signal is modulated by the proof mass displacement and offset. Wu *et al.* [61] carried out a simulation study of 2nd and 3rd EM- $\Sigma\Delta$ accelerometer interfaces with high- Q factor sensing elements ($Q \sim 1000$) and multi-bit force feedback. A pulse density modulation (PDM) was proposed to realize linear multi-bit force feedback. Without considering Brownian and circuit noise, 100dB dynamic range was reported with a 3rd order 3-bit EM- $\Sigma\Delta$ using an oversampling ratio of 256. Xu *et al.* [62] adopted a distributed feedback and feedforward $\Sigma\Delta$ architecture to design a fully differential 5th-order switched capacitor EM- $\Sigma\Delta$ interface in a standard 0.5 μ m CMOS process for a typical bulk micromechanical accelerometer (Fig. 18(a)) with a Q factor above 40. As shown in Fig. 18(b), a lead compensator with a transfer function of $H_c(z) = 1 - 0.9z^{-1}$ was used to provide sufficient phase lead for high Q sensing elements. As sensing and feedback electrodes are not separated (i.e. collocated sensing and feedback), the interface circuit operated in distinct phases: reset, charge sensing, sampling and electrostatic feedback phase. The measured noise floor was lower than 200ng/ $\sqrt{\text{Hz}}$ with a sampling clock of 250kHz. The input range was limited to ± 1.2 g, and the achieved DR was 136dB at 1Hz. The sensitivity, nonlinearity, and bias instability of this EM- $\Sigma\Delta$ accelerometer were 1.896V/g, 0.15%, and 18 μ g, respectively.

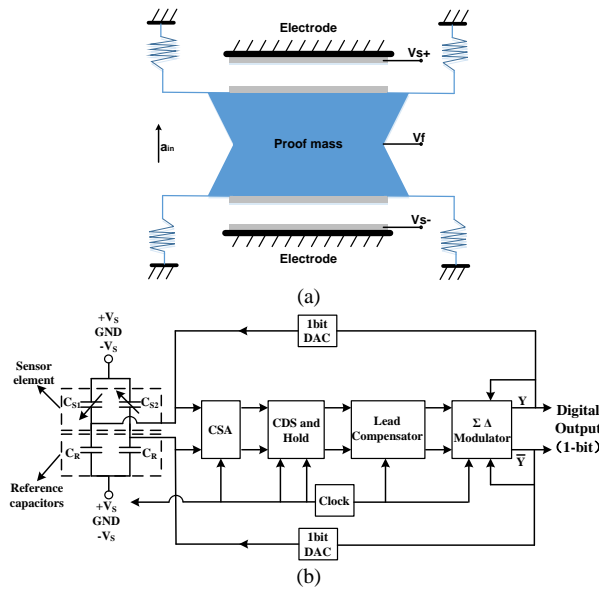


Fig. 18. (a) Model of the accelerometer sensing element (b) Block diagram of the fully-differential SC EM- $\Sigma\Delta$ M closed-loop system proposed by Xu *et al.* From [62].

In [63], a comparison with commercially available capacitive MEMS accelerometers was provided. Many mid-to-high performance MEMS accelerometers are today commercially

available and reach tactical grade performance. However, penetrating the inertial navigation grade market faces competition from established technologies based on macroscopic electro-mechanical servo-accelerometers, such as the Honeywell Q-Flex^R accelerometer series. Employing standard CMOS processes, the size and power consumption of EM- $\Sigma\Delta$ M accelerometers can be significantly improved and enable the production of smart devices for volume inertial navigation markets. A comparison of the main features of published single-loop EM- $\Sigma\Delta$ M force feedback accelerometers and a Q-Flex^R 2000-030 accelerometer is shown in Table I, which also summaries various EM- $\Sigma\Delta$ M interface CMOS IC circuits.

C. MASH $\Sigma\Delta$ M accelerometers

As discussed above, increasing the order of single loop modulators has stability constraints and can only operate with a lower FS acceleration input level compared with a 2nd-order EM- $\Sigma\Delta$ M, otherwise the system will be overloaded and become unstable [30, 59]. An overload recovery mechanism was reported in [58] but added complexity to the system and required additional hardware. Almutairi and Kraft [64, 65] performed a comparative study of two 4th-order EM- $\Sigma\Delta$ M continuous-time interface architectures implemented on a PCB:

TABLE I

SUMMARY OF REPORTED SINGLE-LOOP EM- $\Sigma\Delta$ M ACCELEROMETERS AND HONEYWELL Q-FLEX ACCELEROMETER

Authors	EM- $\Sigma\Delta$ M architectures	FS range and Q factor	Noise floor with bandwidth, f_s	DR within bandwidth	Bias Instability and Sensitivity	CMOS process, Interface IC chip's size	IC core voltage, Power consumption
Henrion <i>et al.</i> [38]	2 nd -order	0.1g, Vacuum	10 μ g/ \sqrt Hz, –	120dB	–, 1V/g	–	–
Boser <i>et al.</i> [39-41]	2 nd -order	\pm 5g, ~1	1.6mg/ \sqrt Hz with 50Hz, 500kHz	50dB (50Hz)	–, –	–	–
Lemkin <i>et al.</i> [42]	2 nd -order	\pm 18g, 2~3 \times 10 ³	110-990 μ g/ \sqrt Hz, 500kHz	70~80dB (100Hz)	–, –	2 μ m, 28mm ²	5V, 135mW
Najafi <i>et al.</i> [43,44]	2 nd -order	\pm 1.35g, ~16	1.5 μ g/ \sqrt Hz with 1kHz, 1MHz	>120dB	–, 0.96V/g	0.5 μ m, 6.24mm ²	5V, 7.2mW
Smith <i>et al.</i> [26]	3 rd -order	\pm 1g, –	1 μ g/ \sqrt Hz with 300Hz, 80kHz	–	–, –	2 μ m, 6.6mm ²	5V, 13.5mW
Wu <i>et al.</i> [45, 61]	3 rd -order, 3-bit quantization	5g, 1000	4.5 μ g/ \sqrt Hz with 2kHz, 1MHz	100dB	–, 0.13V/g	–	–
Kajita <i>et al.</i> [46]	3 rd -order, 3-level force feedback	–, –	–, –	–	–, –	–	–
Petkov <i>et al.</i> [23]	4 th -order, feed-forward	–, –	150 μ g/ \sqrt Hz with 100Hz, 850kHz	–	–, –	0.5 μ m, 0.9mm ²	5V, 13mW
Amini <i>et al.</i> [47, 48]	4 th -order, CIDF	–, 0.3	4 μ g/ \sqrt Hz with 500Hz, 40kHz	95dB (20Hz)	2~8 μ g (12h), 10V/g	0.5 μ m, 2.25mm ²	3V, 4.5mW
Dong <i>et al.</i> [49, 51]	5 th -order, CIDF	\pm 1g, 0.41	32 μ g/ \sqrt Hz with 1kHz, 125kHz	–	–, –	PCB	–
Chen <i>et al.</i> [52]	6 th -order, CIDF	\pm 6g, Vacuum	15 μ g/ \sqrt Hz with 500Hz, 132kHz	–	–, 0.96V/g	PCB	–
Akin <i>et al.</i> [53]	4 th -order, feedforward with unconstrained	\pm 40g, <10	6 μ g/ \sqrt Hz with 250Hz, 1.08MHz	131.9dB (1Hz)	6.4 μ g, –	0.35 μ m, <4mm ²	3.3V, 16.5mW
Pastre <i>et al.</i> [54,55]	5 th -order with CIDF	\pm 11g, –	1.15 μ g/ \sqrt Hz with 300Hz, 1MHz	139.6dB (1Hz)	0.1mg (24h), –	0.6 μ m, 9.7mm ²	3.3V, 12mW
Zwahlen <i>et al.</i> [57-59]	5 th -order with CIDF	\pm 15g, –	1.7~2 μ g/ \sqrt Hz with 300Hz, 1MHz	140dB (1Hz)	10 μ g (600s), –	0.6 μ m, 9.7mm ²	–
Xu <i>et al.</i> [62]	4 th -order, feedforward with multi-feedback	\pm 1.2g, 40	200ng/ \sqrt Hz with 300Hz, 250kHz	136dB (1Hz)	18 μ g, 1.896V/g	0.5 μ m, 7.8mm ²	7V, 23mW
Honeywell [60]	Macroscopic electro-mechanical	60g, –	3 μ g/ \sqrt Hz with 500Hz, –	>150dB (1Hz)	0.1mg (24h), –	–	–

i) a MASH2-2 architecture and ii) a single loop 4th-order CDF $\Sigma\Delta$ architecture. Both architectures improved the bandwidth, dynamic range and linearity compared to an open loop configuration. The results demonstrated that the advantages of an MASH2-2 interface compared to a single loop, high-order interface were inherent stability and high overload input level, due to the use of lower order $\Sigma\Delta$ loops in the individual stages. However, the single loop EM- $\Sigma\Delta$ architecture confirmed its superior immunity to fabrication tolerances as the SNR degradation was negligible for a random variation of the accelerometer sensing element parameters up to about 12%. For the same values the MASH2-2 interface performance degraded by approximately 10dB. The basic system level diagram and schematic of the MASH2-2 interface circuit are shown in Fig. 19(a) and (b), respectively. For the capacitive accelerometer used in this study the measured noise floor of the MASH2-2 interface was about $47\mu\text{g}/\sqrt{\text{Hz}}$ (-110dB), which improved the performance of a 2nd-order EM- $\Sigma\Delta$ interface by 20dB. The FS input range of the MASH2-2 interface was $\pm 1.5\text{g}$ whereas the 4th-order single loop interface was less than $\pm 1\text{g}$ [37, 66].

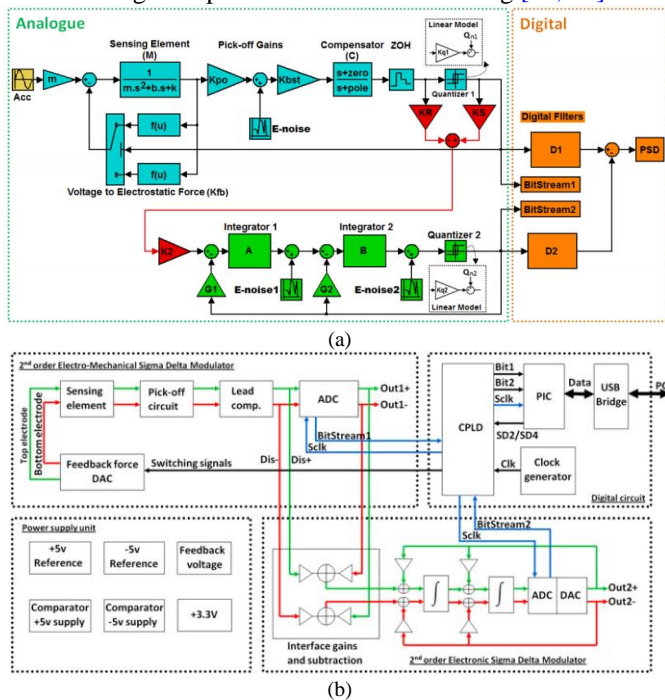


Fig. 19. (a) A 4th-order MASH2-2 interface: The first loop comprised the sensing element, whereas the second loop was purely electronic; the output bitstreams of the two loops were combined by two digital filters [64, 65]. (b) Schematic diagram of a continuous-time MASH2-2 interface circuit implemented on a PCB [37, 66].

An interesting variant of the MASH architecture using a dual quantization technique was recently reported by Almutairi *et al.* [67, 68]; this architecture was described as an electromechanical MASH2-0 interface and applied to a capacitive accelerometer. The system consisted of the sensing element followed by a pick-off circuit and then interfaced to a multi-bit ADC for quantization. This was followed by a digital compensator and a single-bit quantizer controlling the electrostatic pulse feedback force to close the loop. Both quantization noise sources generated by the two quantizers were shaped by the 2nd-order mechanical loop filter. However, as the single-bit quantization noise was in digital format and was

considerably greater than of a multi-bit ADC quantizer, it could directly be cancelled by a digital filter without further cascaded $\Sigma\Delta$ loops, reducing the complexity of the digital filter. The system-level view of the MASH2-0 interface is illustrated in Fig. 20. The system was studied by Simulink modeling and a hardware implementation on a FPGA. The MASH2-0 interface shared the benefits of a MASH2-2 architecture of having inherent stability, a high overload input level, and a high dynamic range compared with a single loop architecture. Furthermore, the MASH2-0 interface benefited from a considerably simpler architecture and implementation, while achieving a higher dynamic range and a higher SNR compared with a MASH2-2 and a 4th-order single-loop EM- $\Sigma\Delta$ architecture. The MASH2-0 interface performance was experimentally compared with a MASH2-2 and a 4th-order single-loop EM- $\Sigma\Delta$ architecture, which were both implemented for an identical accelerometer sensing element on the same PCB board by programming the FPGA accordingly. The results in Fig. 21 indicate that the MASH2-2 and 4th-order single-loop architectures achieved noise floors around $0.63\text{mg}/\sqrt{\text{Hz}}$ (-110dB), while the noise floor of the MASH2-0 was less than $63\mu\text{g}/\sqrt{\text{Hz}}$ (-130dB) within a bandwidth of 1 kHz. Three hours zero-output data was gathered and the bias instability was reported as $20\mu\text{g}$ at an integration time of 40s. Table II shows a summary of the MASH architecture EM- $\Sigma\Delta$ accelerometers discussed above.

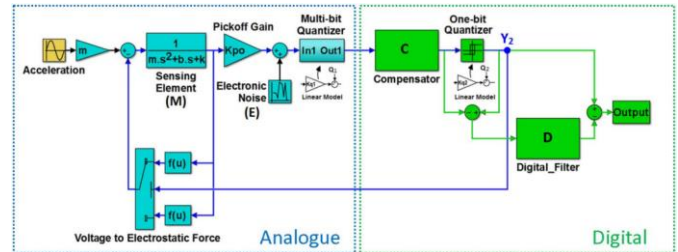


Fig. 20. Block diagram of the MASH2-0 EM- $\Sigma\Delta$ accelerometer proposed by Almutairi *et al.* From [68].

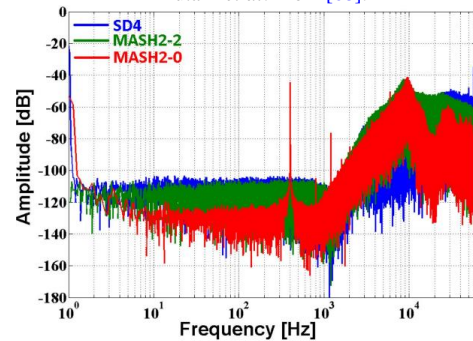


Fig. 21. Measured noise shaping of the 4th-order single-loop, MASH2-2, and MASH2-0 are -110dB, -110dB, and -130dB, respectively. From [68]

TABLE II

THE SUMMARY OF PUBLISHED MASH ARCHITECTURE EM- $\Sigma\Delta$ ACCELEROMETER

Author	MASH architecture	FS range and DR	Noise floor with bandwidth, f_s , Sensitivity	Bias Instability, Q factor
Almut airi <i>et al.</i> [37]	MASH 2-2	$\pm 1.5g$, 106dB	$47\mu g / \sqrt{Hz}$ with 1kHz, 125kHz, -	-, ~ 10
Almut airi <i>et al.</i> [68]	MASH 2-0	$\pm 20g$, 118dB	$63\mu g / \sqrt{Hz}$ with 1kHz, 131kHz, -	$20\mu g$ (3h), ~ 3

IV. ELECTROMECHANICAL $\Sigma\Delta$ VIBRATORY RATE GYROSCOPE

A. Low-pass EM- $\Sigma\Delta$ gyroscopes

A micromachined vibratory rate gyroscope is in the sense mode essentially an acceleration sensor that measures Coriolis acceleration. Fig. 22(a) shows a typical block diagram of a MEMS gyroscope. There are two orthogonal vibration modes: drive (x) and sense (y) mode, with two corresponding control loops for each mode. The Coriolis force transfers energy from the drive to the sense mode of a two degree of freedom resonant mechanical structure. In the drive mode, the proof mass is electrostatically driven to oscillate with a constant amplitude and frequency. This oscillation is usually controlled by a closed loop control system; for example, a phase-lock-loop (PLL) and automatic gain control (AGC) [69-74]. To increase the bandwidth, reduce nonlinearity and improve the immunity to fabrication tolerances, it is of considerable advantage to include the sense mode of a gyroscope in a force feedback control loop. Jiang *et al.* [75] first reported a 2nd-order EM- $\Sigma\Delta$ CMOS interface for a capacitive z-axis gyroscope, which is depicted in Fig. 22(b). As the sense mode of the gyroscope is embedded as a 2nd-order low-pass EM- $\Sigma\Delta$ force feedback loop (similar to 2nd-order EM- $\Sigma\Delta$ accelerometers) the SNR has an upper limit and can be improved only by increasing the oversampling frequency f_s . The gyroscope achieved a noise floor of 3 %s / \sqrt{Hz} at atmospheric pressure. Petkov *et al.* [23] proposed a 4th-order low-pass feed-forward $\Sigma\Delta$ gyroscope, operating at a sampling rate of 850kHz and achieving a noise floor of 1 %s / \sqrt{Hz} at atmospheric pressure.

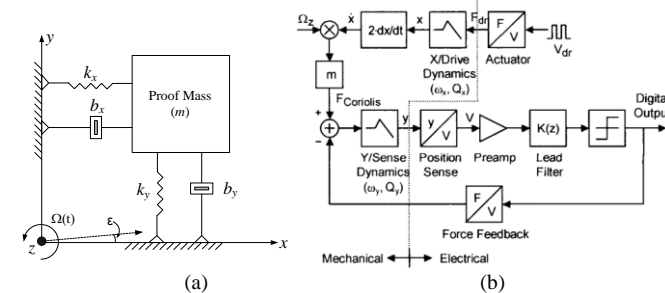


Fig. 22. (a) Systematic model of a Z-axis vibratory gyroscope (b) 2nd-order $\Sigma\Delta$ Z-axis gyroscope: the mechanical element in the sense mode is used as a noise-shaping filter in a one-bit $\Sigma\Delta$ converter with architecture similar to a 2nd-order $\Sigma\Delta$ accelerometer [75].

Rodjergard *et al.* [76] first implemented a low-pass 5th-order EM- $\Sigma\Delta$ digital interface on an ASIC chip for the SAR10 microgyroscope sensing element developed by SensoNor [77];

the system diagram is depicted in Fig. 23. The interface circuit comprising a high performance capacitive readout amplifier, 5th-order $\Sigma\Delta$ and analog feedback recovery circuits. Further digital building blocks including the demodulation circuitry, filtering and timing were implemented on an FPGA. The interface ASIC and the FPGA communicated by digital $\Sigma\Delta$ bit-streams processed by decimation filters. The interface ASIC was built up from two identical signal paths, one for the excitation loop and one for the detection loop. Each loop consisted of a charge amplifier, $\Sigma\Delta$ building blocks, a digital feedback implementation with a $\Sigma\Delta$ feedback signal and a recovery circuit for the feedback signal. The gyroscope had a noise floor of 0.003 %s / \sqrt{Hz} and an Allan variance bias instability of 3.2 %h.

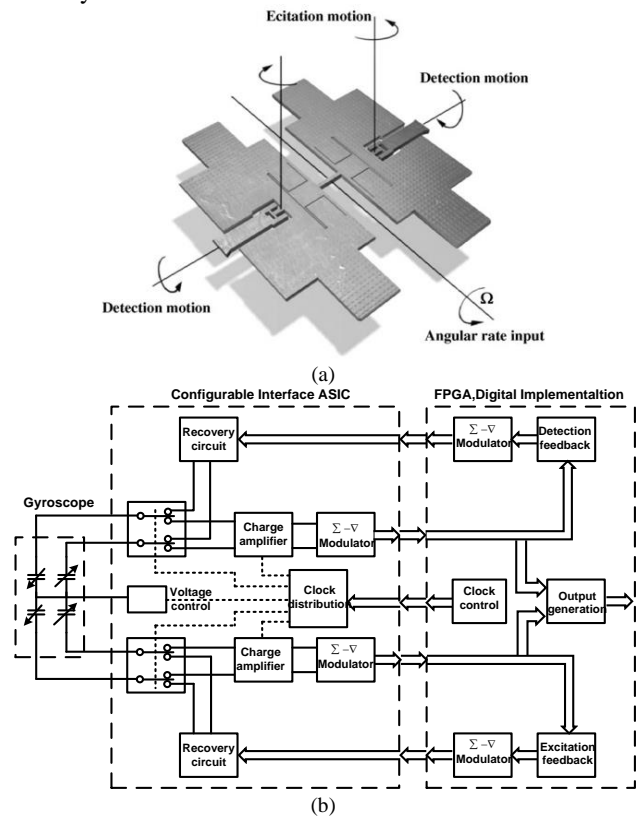


Fig. 23. (a) Functional principle of the SAR10 butterfly structure microgyroscope sensing element [77]. (b) A fifth-order $\Sigma\Delta$ digital interface proposed by Rodjergard *et al.* From [76].

Raman *et al.* [78, 79] proposed a DT EM- $\Sigma\Delta$ interface for both the drive (primary) and sense (secondary) modes of a dual-frame vibratory gyroscope. The analog C/V interface electronics and the digital parts were implemented on a separate CMOS chip and an FPGA, respectively. For the drive oscillation in Fig. 24(a), the displacement was measured by a continuous-time C/V circuit and converted to the digital domain by a conventional $\Sigma\Delta$ ADC. The phase shifter and amplitude controller were realized in the DT domain. The driving force signal was obtained from a digitally controlled quadrature oscillator (DCO). Then, the multi-bit digital signal was converted into a one-bit signal with a digital $\Sigma\Delta$ and used for feedback actuation. An error compensation building block was also added to the frequency tracking loop to compensate for parasitic electrical coupling. For the sense mode, as shown in

Fig. 24(b), the readout circuit was based on an optimal single-bit unconstrained mixed-feedback $\Sigma\Delta$ force-feedback structure, replacing the front-end resonator stage of an unconstrained electrical $\Sigma\Delta$ with the mechanical sensor without requiring access to the signal at the internal node of the sensing element. Therefore, the EM- $\Sigma\Delta$ force-feedback loop did not require a compensation filter to retain stability. The resulting overall gyroscope system had a noise floor of 0.025 %/√Hz with a bandwidth of 100Hz and a linearity better than 0.25 % in a range of ±150°.

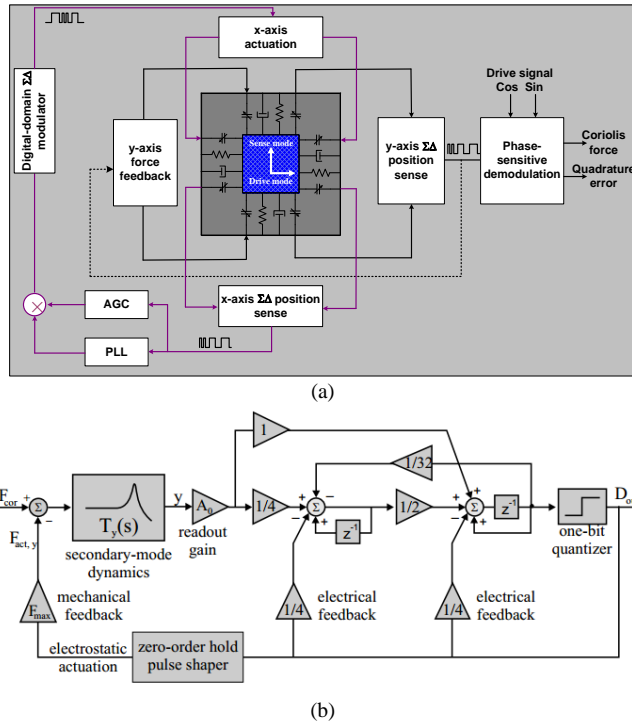


Fig. 24. (a) System level overview. (b) A unconstrained feed-forward EM- $\Sigma\Delta$ interface with a electrical resonator providing a notch in the NTF at the operating frequency of the gyroscope. From [78, 79].

When comparing DT and CT EM- $\Sigma\Delta$ interface implementations, CT interfaces suffer less from noise folding, consequently the noise floor is inherently lower [25]. The requirements on the gain-bandwidth specifications for the amplifiers in CT implementations are more relaxed leading to lower power consumption compared to their DT-counterparts [25]. Rombach *et al.* [80] described a novel modulated single loop 4th-order CT low-pass EM- $\Sigma\Delta$ gyroscope interface with feed-forward architecture having a high tolerance to parameter variations from sensor fabrication. As shown in Fig. 25, two modulation-stages were added to the EM- $\Sigma\Delta$ force feedback loop. This allowed reducing the sampling frequency f_s of the $\Sigma\Delta$ to the drive resonance frequency of the gyroscope. However, the approach was only demonstrated in simulation for a gyroscope sensing element with a moderate sense mode Q factor of 500.

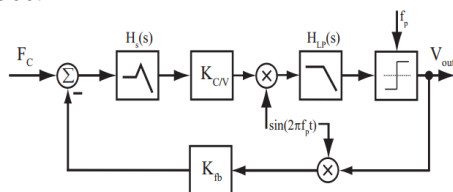


Fig. 25. A novel modulated low-pass EM- $\Sigma\Delta$ gyroscope interface designed by Rombach *et al.* [80]. The modulation-stages allowed reducing the sampling frequency to the drive mode resonance frequency.

Using a 0.18 μ m high-voltage CMOS process, in 2011 Elsayed *et al.* [81] from Si-Ware Systems (SWS) [82] launched a commercial interface ASIC chip based on the architectures presented by Raman [79] and Petkov [23]. As shown in Fig. 26, a 4th-order EM- $\Sigma\Delta$ force-feedback loop with a feed-forward $\Sigma\Delta$ topology and a feed-back branch was implemented in an ASIC suitable for CT feedback operation. The output of the $\Sigma\Delta$ sense loop was filtered and decimated using a programmable decimation band-pass-filter, centered around the gyroscope resonance frequency. The filter had a bandwidth of 200Hz and attenuated the noise of the sense output signals, before multiplying it with the drive velocity signal for demodulation. Hence, mixing and down conversion of the quantization noise to the band of interest was not necessary. As the poles and zeros of the band-pass-filter scale with the sampling frequency, the center frequency could be correctly tuned with variations of the gyroscope resonance frequency. This ASIC chip was fabricated and combined with a MEMS gyroscope in a single Leadless-Chip-Carrier (LCC) package. The gyroscope used mode-matching [83] and achieved a noise floor of 1m %/√Hz over a 200Hz bandwidth, a linearity of 0.26% and a FS range of ±400 % [81].

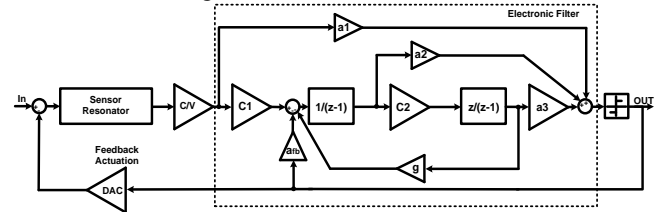


Fig. 26. Elsayed *et al.* implementing a 4th order feed-forward with feedback branch $\Sigma\Delta$ topology for the sense mode of a gyroscope. From [81].

B. Band-pass EM- $\Sigma\Delta$ gyroscopes

The aforementioned architectures are all principally low-pass EM- $\Sigma\Delta$ force feedback architectures, having achieved remarkable performance with a bias instability of down to 3.2 %h. However, their performance is limited because of the characteristics of a low-pass EM- $\Sigma\Delta$, mainly as the required sampling frequency is relatively high compared to the bandwidth of a typical MEMS silicon gyroscope [84]. As the output characteristics of a vibratory rate gyroscope is a narrow band amplitude modulated signal, a band-pass EM- $\Sigma\Delta$ force feedback architecture is an interesting alternative for the interface architecture. The main advantage of this approach is that significantly lower sampling frequencies can be used. Similar principles as for the design of electronic $\Sigma\Delta$ band-pass ADC lend themselves to be applied to MEMS vibratory gyroscopes. The vibratory gyroscope is usually designed to have a high quality factor in the drive mode (Q_x) and the sense mode (Q_y), requiring active resonant mode matching control. The maximum sensitivity is achieved when the resonant frequencies of the two modes are matched [83]. The system in [83] had a bandwidth of less than 1Hz, but perfect frequency matching is practically not achievable. Dong *et al.* [25] presented a comparative study of a high-order low-and band-pass EM- $\Sigma\Delta$ gyroscope while assuming a resonant

frequency mismatch of the two modes by $\pm 5\%$. The low-pass EM- $\Sigma\Delta$ gyroscope had about 15dB signal amplitude loss due to the mode frequency mismatch while no signal amplitude degradation was observed in the band-pass EM- $\Sigma\Delta$ gyroscope. Ezekwe *et al.* [29, 85] designed a band-pass EM- $\Sigma\Delta$ architecture for a vacuum operated gyroscope to exploit mode-matching effectively and use pulse density modulated force feedback to achieve a bandwidth well in excess of 50Hz. The overall system diagram is shown in Fig. 27, including the feedback loop to measure the Coriolis force and tune the sense mode resonance frequency to match the drive mode frequency. The same set of electrodes was used for position sensing and feedback using time multiplexing to separate the signals. The positive feedback compensator is used to guarantee stability and ensure sufficient shaping of the quantization noise [28]. The interface circuit was fabricated in a 0.35 μ m CMOS process and resulted in a 0.004 $\%s / \sqrt{\text{Hz}}$ noise floor over a 50Hz band. The system sampling rate was 32 times the drive resonance frequency, approximately 480kHz.

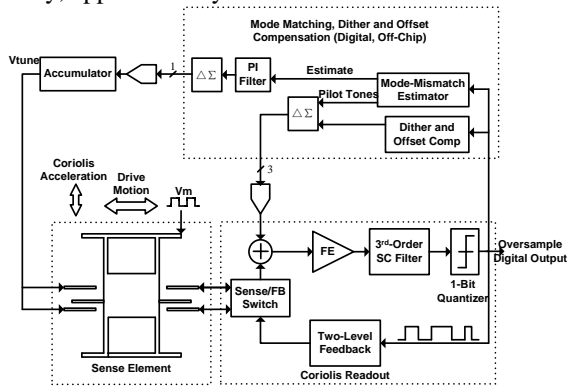


Fig. 27. Band-pass EM- $\Sigma\Delta$ with mode-matching interface proposed by Ezekwe *et al.* From [85].

Northemann *et al.* [86-88] demonstrated a MEMS gyroscope system with a band-pass $\Sigma\Delta$ in both drive and sense modes, as illustrated in Fig. 28. The drive loop used a 4th-order DT band-pass $\Sigma\Delta$ -DAC to reduce the analog circuit complexity by restricting the driving voltage to two fixed potentials. The input signal of the DAC was a square wave signal at the resonant frequency provided by a PLL, and the amplitude controlled by the AGC. For the sense mode, an excess loop delay compensator and a 2nd-order electrical band-pass filter were implemented in the CT domain or using an FPGA emulating CT behavior. The spectrum of the output bitstream in [86] illustrates the combined noise shaping effect from the sensing element transfer function and the additional electrical bandpass filter with a center frequency at the drive resonance frequency. Measurement results showed an in-band noise below -60dB of FS (FS was 1019 $\%s$) in a bandwidth of 100Hz; this is equivalent to a noise floor of 0.1 $\%s / \sqrt{\text{Hz}}$.

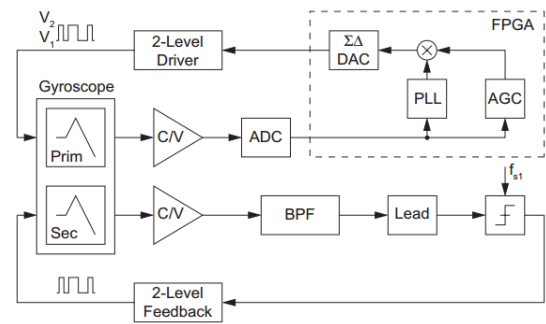


Fig. 28. Block diagram of Northemann's EM- $\Sigma\Delta$ interface control loops for drive and sense modes of a MEMS gyroscope. From [86-88].

Dong *et al.* [89-91] presented a novel 6th-order CT, band-pass EM- $\Sigma\Delta$ force-feedback control system for the SAR10 butterfly structure microgyroscope [77]; the system diagram is depicted in Fig. 29. The sensing element acted as a mechanical resonator, sensing and feedback electrodes were separated. The displacement was converted to a voltage through a capacitive pick-off circuit with conversion gain K_{po} . Two electronic resonators were cascaded to provide additional noise shaping. The multi-feedback topology had to be adopted through a half-return-zero (HRZ) DAC and a return-zero (RZ) DAC, due to the excess loop delay in continuous-time $\Sigma\Delta$ [92]. The local feedback loop gains K_{rz} and K_{hrz} were used to provide multi-feedback waveforms to maintain the same frequency response. A clocked one-bit quantizer was used to output the bitstream and to control the HRZ and RZ DACs, and also the conversion from voltage to electrostatic feedback force. The preliminary experimental result demonstrated that the CT control system had a noise floor of 0.07 $\%s / \sqrt{\text{Hz}}$ in a 100Hz bandwidth.

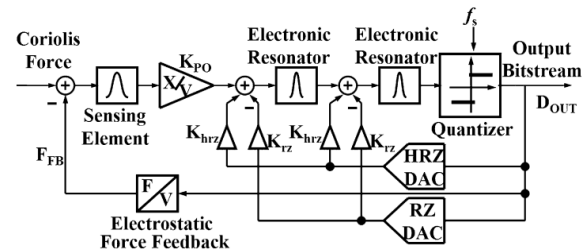


Fig. 29. 6th-order CT band-pass EM- $\Sigma\Delta$ interface for sense mode of gyroscope [91].

Nessler *et al.* [93] used the same pair of capacitors for signal readout and force feedback (collocated sensing and feedback) in a CT band-pass $\Sigma\Delta$ gyroscope using time multiplexing [29, 85]. The concept was based on a modulation of the feedback voltage onto the input common mode of a pick-off C/V charge integrator. The working principle is illustrated in Fig. 30. A feedback voltage V_{fb} was applied to the positive input of the charge integrator. As the open loop gain of the amplifier was very high, a virtual short at the input terminals was generated. A compensation circuit was added at the negative input and therefore the input common mode was modulated without any change of the output voltage. The interface circuit was fabricated in a 0.35 μ m CMOS process and connected via wire bonding to a bulk-micromachined gyroscope provided by the research institute HSG-IMIT. Using mode matching and quadrature compensation, the averaged noise floor was

8m %s / $\sqrt{\text{Hz}}$ over a bandwidth of 40Hz and the bias stability was 16 %h. The system consumed less than 220uA from a 3.3V power supply, which is well suited for battery powered devices.

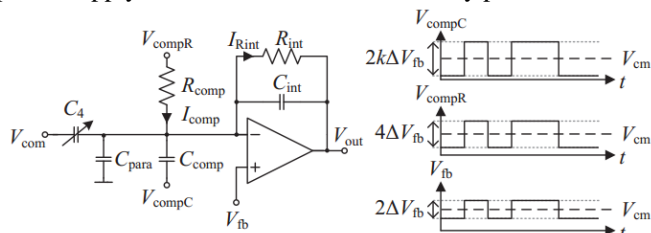


Fig. 30. Concept of CT collocated feedback within the pick-off charge integrator proposed by Nessler *et al.* From [93].

In order to improve the bias instability of EM- $\Sigma\Delta\text{M}$ digital closed-loop gyroscopes, Ismail *et al.* [94] designed a programmable capacitive generic closed-loop force feedback interface ASIC circuit based on 0.18 μm high-voltage CMOS technology. The ASIC circuit included the sense and drive control loop and is illustrated in Fig. 31. The gyroscope together with the ASIC constituted the oscillatory drive loop, and the sense loop required for EM- $\Sigma\Delta\text{M}$ force-feedback closed-loop operation. As the sense mode of gyroscope was an undamped 2nd-order low-pass transfer function, the additional electronic resonator filters produced a notch in the noise transfer function resulting in a 4th band-pass modulator. The gyroscope digital output signal was filtered before demodulation to avoid down conversion of quantization noise in the band of interest. The demodulation output was decimated using a programmable decimation filter which consisted of a cascaded-integrator comb (CIC) filter and a half band filter. The gyroscope system showed a performance with a bias instability of 1 %h and a noise floor of 1.3m %s / $\sqrt{\text{Hz}}$ over a bandwidth of 100Hz. The FS range of the sensor was ± 300 %, while consuming 25mA from a 5V supply.

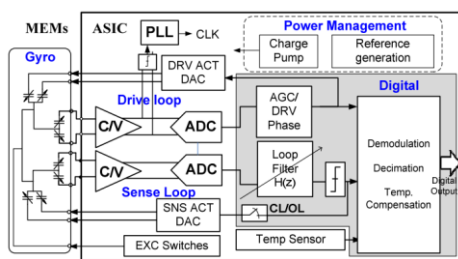


Fig. 31. Ismail *et al.* presented a generic high performance interface ASIC with $\Sigma\Delta\text{M}$ control loop for MEMS gyroscopes. From [94].

V. PARAMETER OPTIMIZATION OF EM- $\Sigma\Delta\text{M}$ FORCE FEEDBACK SYSTEMS

The design of high-order EM- $\Sigma\Delta\text{M}$ for MEMS inertial sensors is complex as the highly nonlinear characteristics of the single-bit quantizer makes conventional system analysis difficult. Furthermore, ensuring overall system stability is challenging. The parameters of the front-end interface circuit, the electronic part of the $\Sigma\Delta\text{M}$ loop filter and the feedback gain have to be optimized to achieve closed-loop stability and, concurrently, maximize performance of the designed accelerometer or gyroscope (sensitivity, linearity, dynamic range, bias instability, etc.). There is no precise analytic approach of EM- $\Sigma\Delta\text{M}$ closed-loop system design due to its

nonlinear components, such as the quantizer, conversion from voltage to electrostatic force, etc. The designer has to resort either to an approximate linearized model followed by lengthy system level simulations or use a genetic algorithm with a non-linear, parametrized model.

Approximated, linearized analytical models for $\Sigma\Delta\text{M}$ were described for example in [95] and employed extensively in the design of electromechanical $\Sigma\Delta\text{M}$ to predict performance [75, 78-79, 86-91]. It enables the use of linear control system analysis and provides valuable insights regarding stability and noise performance of the EM- $\Sigma\Delta\text{M}$. Fig. 32(a) shows the linear model of a generic, all-electronic $\Sigma\Delta\text{M}$ for analog to digital conversion. It consists of an electronic loop-filter and a binary quantizer. The dominant noise sources in the system are the electronic noise from the first integrator of the loop filter (n_{el}^2) and the quantization error (n_{q}^2). The noise contribution from the later stages of the loop-filter is negligible due to the high in-band gain of the first integrator. Fig. 32(b) shows the linear model of an EM- $\Sigma\Delta\text{M}$. The continuous-time transfer function of the mechanical sensing element is represented by its discrete-time equivalent, $H_{\text{m}}(z)$, which includes the sampling operation carried out in the electronic interface as well as the implicit zero-order hold (ZOH) function realized by the feedback path [20, 96]. The three main noise sources are mechanical (Brownian) noise from the sensing element, electronic noise from the interface and quantization noise from the quantizer. In the linear model, the single-bit quantizer is replaced with a variable, signal-dependent gain and an additive noise source. In a linear system the noise contributions can be analyzed separately and the results superimposed. The EM- $\Sigma\Delta\text{M}$ closed-loop systems are conditionally stable. An approach described to find the optimal linear system parameters was based on a root locus approach [36] and a stability criteria for the noise transfer function (NTF gain < 1.5) [25]. However, this had to be followed by extensive system level simulations including the nonlinear effects.

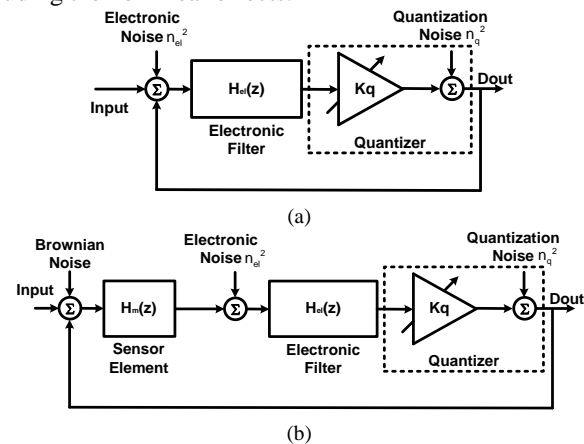


Fig. 32. Linearized $\Sigma\Delta\text{M}$ models: (a) electronic modulator, (b) electromechanical modulator. From [96, 97].

Linearized analytical models are of limited use in predicting the performance and stability of electromechanical $\Sigma\Delta\text{M}$, in particular for high-order electromechanical $\Sigma\Delta\text{M}$ for which stability is a particular concern and the linearization of the quantizer is a less reasonable approximation [97]. Furthermore, there is a nonlinear term due to the dependence of the feedback

force on the proof mass position which can have implications on stability and performance and cannot be captured by a linear model [49]. Wilcock and Kraft [98] proposed a novel design methodology using non-linear simulation models for EM- $\Sigma\Delta$ and a genetic algorithm (GA) followed by a Monte Carlo statistical variation analysis. This design methodology is represented by the flow-chart shown in Fig. 33, which is applicable for any topology with any order. It was demonstrated for a low-pass EM- $\Sigma\Delta$ accelerometer and a band-pass EM- $\Sigma\Delta$ gyroscope.

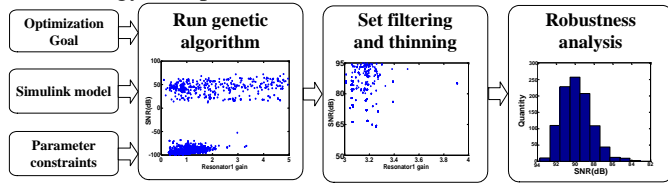


Fig. 33. Generic process flow for the GA-based design algorithm [98].

The first step in the design process is to develop a parametrized Simulink model of a general suitable EM- $\Sigma\Delta$ architecture (based either on a purely electronic A/D $\Sigma\Delta$ or a novel architecture). Secondly, one or several goal parameters for the GA to optimize as an objective have to be defined. For EM- $\Sigma\Delta$ MEMS inertial sensors typical objectives are: i) the SNR calculated from a Fast Fourier transformation (FFT) of the output bitstream and ii) the residual motion of the proof mass which should be significantly smaller compared to an open loop sensor. An unstable system can be identified from a negative SNR, thus optimizing towards high SNR solutions ensures that stability is addressed as part of the GA. The ratio between open loop and $\Sigma\Delta$ closed loop proof mass deflection provides a measure of how well the sensing element is controlled by the electrostatic feedback force, and gives insight into the improvement in dynamic range compared to the open loop case. The Monte Carlo robustness analysis following the GA is crucial, giving confidence in a design and ensuring manufacturability. With this approach several optimized high-order EM- $\Sigma\Delta$ accelerometers and gyroscopes were designed and implemented [37, 52, 99]; two Simulink models from these publications are shown in Fig. 34. As shown in Fig. 35, the simulated output spectrum of an optimized 6th-order BP- $\Sigma\Delta$ gyroscope has better band-pass characteristics when compared to a non-optimized system. Chen *et al.* [100] also extended the GA optimization not only to a high-order EM- $\Sigma\Delta$ interface for the sense mode, but also to the drive mode self-oscillation control loop of a gyroscope. The described GA optimization combines finding a stable EM- $\Sigma\Delta$ system with maximum SNR and minimal proof mass deflection for gyroscopes or accelerometers.

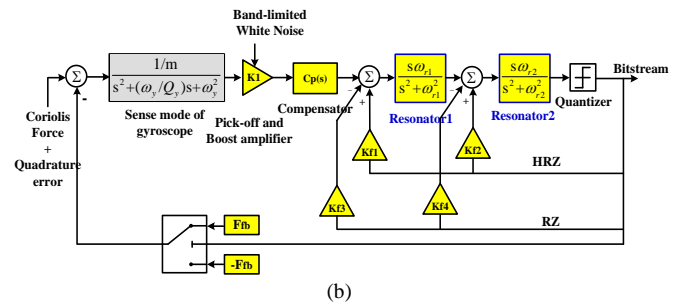
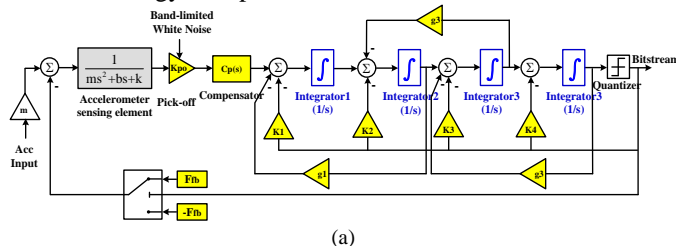


Fig. 34. Simulink model of the high-order EM- $\Sigma\Delta$ interface for (a) accelerometer [52] and (b) gyroscope [99]. Parameters that are changed by the GA are highlighted in yellow.

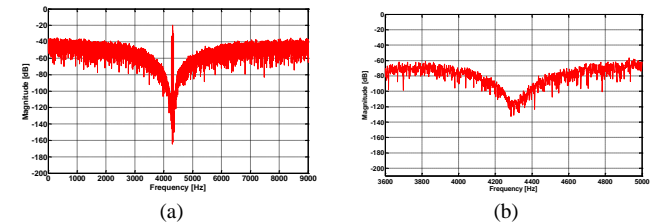


Fig. 35. The output band-pass characteristics of an optimized (a) and non-optimized (b) 6th-order BP- $\Sigma\Delta$ gyroscope by Chen *et al.* From [99].

Table III shows all published EM- $\Sigma\Delta$ sense mode force feedback closed-loop gyroscopes from 2000 to date. It is apparent that the academic research and development made impressive and steady progress. Combined with advanced CMOS technology and various calibration techniques such as mode-matching, high performance EM- $\Sigma\Delta$ gyroscopes exhibit low power consumption are now becoming mainstream.

VI. DISCUSSION AND FUTURE PROSPECTS

The extremely small output signal of the capacitive MEMS sensing element is a major challenge in inertial sensor design. Typically, it is a differential capacitive signal that has to be sensed by a low-noise charge amplifier and provides a measure of the proof mass position [1]. A $\Sigma\Delta$ introduces a quantization error as additional noise source. The main goal of applying $\Sigma\Delta$ modulation to inertial sensors is to retain the advantages of feedback and digitization without compromising the resolution of the analog front-end. The increase in the order of a EM- $\Sigma\Delta$ interface leads to higher order quantization error filtering. 4th, 5th and 6th-order EM- $\Sigma\Delta$ interfaces proved to achieve better SNR than 2nd-order architectures in various published studies. However, it cannot be concluded in general that the performance improvement of MEMS inertial sensors is a result of increasing the order of EM- $\Sigma\Delta$ interfaces. A further increase in the order leads to problems in terms of system stability, complexity and low overload conditions in realistic circuit implementations. It is therefore not expected that orders higher than six are a sensible choice for EM- $\Sigma\Delta$ interfaces.

Some capacitive inertial sensing elements use the same electrodes for sensing and feedback (collocated electrode arrangement), while others use separate dedicated electrodes (non-collocated electrode arrangement) [28]. One of the major challenges in the design EM- $\Sigma\Delta$ force feedback interface circuits is the cross-talk between the feedback and sense signals.

TABLE III
SUMMARY OF EM- $\Sigma\Delta$ SENSE MODE FORCE FEEDBACK CLOSED-LOOP GYROSCOPE

Authors	EM- $\Sigma\Delta$ architectures	Q_y (sense mode)	Noise floor with f_s	FS and bandwidth	Bias Instability and sensitivity	CMOS process, Interface IC chip's size	IC core voltage, Power consumption
Jiang <i>et al.</i> [75]	2 nd -order	2.6	3 %s/ $\sqrt{\text{Hz}}$, 1MHz	1000 %s, -	-, -	2 μm , 20.25mm ²	5V, 50mW
Petkov <i>et al.</i> [23]	4 th -order feed-forward r	<20	1 %s/ $\sqrt{\text{Hz}}$, 850kHz	-, -	-, -	0.5 μm , 0.9mm ²	5V, 18mW
Rodjégard <i>et al.</i> [76]	Low-pass 5 th -order	200~250	0.003 %s/ $\sqrt{\text{Hz}}$, 2MHz	-, -	3.2 %h, -	-, 9.6mm ²	-
Raman <i>et al.</i> [78-79]	4 th -order unconstrained	10~15	0.025 %s/ $\sqrt{\text{Hz}}$, 400kHz	1100 %s, >100Hz	0.023 %s, 7.73 LSB/ %s	0.6 μm with HV, 9mm ²	5V, 3.05mW
Elsayed <i>et al.</i> [81]	4 th -order feed-forward with feedback	-	1m %s/ $\sqrt{\text{Hz}}$	± 400 %s, 200Hz	-, -	0.18 μm with HV, 28mm ²	5V, 320mW
Ezekwe <i>et al.</i> [29, 85]	4 th -order feed-forward	Vacuum	4m %s/ $\sqrt{\text{Hz}}$	-, 50Hz	-, -	0.35- μm , 0.32mm ²	3V, 9.9mW
Dong <i>et al.</i> [89-91]	Band-pass 6 th -order multi-feedback	200~250	0.07 %s/ $\sqrt{\text{Hz}}$, 40kHz	-, 100Hz	-, -	PCB	-
Northemann <i>et al.</i> [86-88]	Band-pass 4 th -order multi-feedback	100	0.1 %s/ $\sqrt{\text{Hz}}$, 8 ω_d	1019 %s, 100Hz	-, -	-	-
Nessler <i>et al.</i> [93]	Band-pass 4 th -order	-	8m %s/ $\sqrt{\text{Hz}}$	40Hz	16 %h	0.35 μm , 1.68 mm ²	3.3V, 770 μW
Ismail <i>et al.</i> [94]	Band-pass 4 th -order	-	1.3m %s/ $\sqrt{\text{Hz}}$	± 300 %s, 100Hz	1 %h, 1×10^4 LSB/ %s	0.18 μm HV, 12mm ²	5V, 25mW
Chen <i>et al.</i> [99,100]	Band-pass 6 th -order multi-feedback	114	0.07 %s/ $\sqrt{\text{Hz}}$, 32kHz	± 220 %s, 110Hz	34 %h, 3.8 LSB/ %s	PCB	-

The feedback signal occurs in the form of pulses, and thus easily couples into the sense signal through parasitic capacitances inherent to the micromachined sensing element. Fig. 36 shows a block diagram of a capacitive accelerometer sensing element with non-collocated feedback and sensing (i.e. the sensing and feedback capacitors are separated). If the feedback electrode to the top of the proof mass (C_{fb_top}) is energized, and the electrode to the bottom of the proof mass (C_{fb_bot}) is grounded, a larger coupling signal is fed to the top sense capacitor (C_{s_top}) through the parasitic capacitor (C_{fb_tp}) while a smaller coupling signal is fed to the bottom sense capacitor (C_{s_bot}) through the parasitic capacitor (C_{fb_bp}). Due to the difference of the coupled signal amplitudes, the differential output of the pickoff circuit is disturbed, affecting the performance of the EM- $\Sigma\Delta$ force-feedback system. The cross talk signal can be eliminated by using a time multiplexing scheme between the feedback and the sense electrodes, where a fraction of a cycle is used for sensing, the remaining time for force feedback. During the sensing phase, the feedback electrodes are grounded and give the parasitic capacitance enough time to discharge; this is a commonly used approach in CT and DT implementations. In practice, this method does not give the best performance as it introduces extra switching noise and requires the sensing phase to be relatively long, which also degrades the EM- $\Sigma\Delta$ closed-loop performance. Other methods have been reported including modulating the feedback voltage onto the input common mode of a pick-off charge integrator [93], implementing a high pass or band pass filter after the pickoff circuit and filtering out the coupling signals caused by the digital feedback pulses [35].

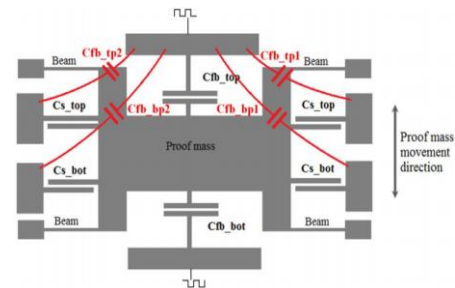


Fig. 36. Simplified model of sensing and feedback electrode arrangement in a accelerometer sensing element including parasitic capacitances C_{fb_xt} [35].

For high performance EM- $\Sigma\Delta$ gyroscopes and accelerometers bias instability, dynamic range, linearity, bandwidth and high integration are the primary performance criteria. With the maturity of high-voltage CMOS technology, the implementation of CT and DT EM- $\Sigma\Delta$ interface circuits with adjustable high feedback voltage is becoming an interesting option. DT EM- $\Sigma\Delta$ interfaces based on dual quantization techniques, with the electronic loop filter implemented on a FPGA, have the advantages of easy debugging and low-temperature sensitivity. Furthermore, innovative control and optimization algorithms for $\Sigma\Delta$ architectures can easily be mapped to a circuit implementation. Chip-level self-testing, self-calibration, temperature compensation and other intelligent functions are relatively easy to add. Mixed signal CMOS analog and digital systems are an important trend for DT EM- $\Sigma\Delta$ interfaces. Many of the reported implementations use DT EM- $\Sigma\Delta$, which are, in contrast to CT implementation, susceptible to noise folding. In addition, the amplifiers in DT circuits typically require higher bandwidth [80, 91]. The main disadvantage of CT EM- $\Sigma\Delta$ interfaces circuit is a higher susceptibility to temperature drift, cross-coupling (especially for PCB implementations), tolerances of resistor and capacitor values,

feedback pulse errors, sensing element fabrication errors, and the challenge to find an optimized architecture. Further research is required to develop self-adaptive real-time optimization techniques suited for EM- $\Sigma\Delta$ interfaces to alleviate the influence of aforementioned issues.

Small size, multi-functionality, high-precision and low cost are the ultimate goals of MEMS inertial sensors. Following the trend in consumer electronics, the application fields of high performance combined multi-axes inertial sensors (dual-axis or tri-axis accelerometers and gyroscopes) are constantly increasing, especially for industrial and military fields. This stimulates interest in the development of combo high performance micro-sensors integrating accelerometers and gyroscopes with other sensors such as resonators for time keeping, magnetometers and barometers on a common substrate to form 9 or 10-DOF sensing microsystems and 6-DOF inertial microsystem units. For automotive applications, for example, a discrete accelerometer and gyroscope add up to about \$13, while the equivalent combo sensor costs about \$11 [2]. Despite the significant advancements already achieved, there still exist several challenges to achieve navigation grade performance; for example vacuum operation is required for high performance gyroscopes and resonators. However, this is contradictory to accelerometers which should be critically damped. EM- $\Sigma\Delta$ interface circuitry can be utilized to not only electrostatically damp the accelerometers, but also for gyroscopes and magnetometers to operate in closed-loop mode [52], hence offer a unified interface and control technology. Future research will address cross-axis sensitivity, pulse density modulated coupling and parameter mismatch of EM- $\Sigma\Delta$ multi-axis inertial sensors. A full system model of the sensors combined on one substrate together with adaptive EM- $\Sigma\Delta$ interfaces including various fabrication tolerances would allow for further improvements of the sensor system performance.

There are several MEMS and semiconductor companies focusing on high performance EM- $\Sigma\Delta$ closed-loop gyroscopes and accelerometers, such as Colibrys S.A. [101], Si-Ware Systems (SWS) [82] and Imego AB [102]. Colibrys is one of the main suppliers of high performance MEMS accelerometers. Their main products include an analog (HS8000, MS9000 and MS9010P) and a digital series. Especially, the EM- $\Sigma\Delta$ digital closed-loop series accelerometers offer excellent scale factor stability over temperature, low bias instability from $-40\text{ }^{\circ}\text{C}$ to $80\text{ }^{\circ}\text{C}$, and matches the performance of the Honeywell Q-Flex 2000-30 [60], which are to date the highest performance inertial navigation grade macroscopic electro-mechanical accelerometers available on the market. Although SWS is a fabless semiconductor company providing ASIC interface circuits for MEMS inertial sensors, their interface ASIC platforms (SWS1110, SWS61111, SWS1120 and SWS1130), are rapidly becoming a key tool in realizing high performance capacitive MEMS accelerometers and gyroscopes. Using a $0.18\mu\text{m}$ high-voltage CMOS process technology, SWS's ultra-low noise EM- $\Sigma\Delta$ closed-loop force feedback gyroscope has already demonstrated a bias instability of 1%

while consuming only 25mA from a 5V supply [94].

Despite the general stated benefits of EM- $\Sigma\Delta$ closed-loop force feedback interfaces that have been described in the above reviewed literature, a rigorous study of comparing open-loop with EM- $\Sigma\Delta$ closed-loop interfaces is still missing. The results in [99] indicate that a band-pass EM- $\Sigma\Delta$ closed-loop interface considerably improves the linearity, bias instability and bandwidth of a MEMS gyroscope when compared to open-loop operation. However, the underlying physical effects and reasons for improvement have not been identified in detail, hence systematically studying the characteristics of open-loop and EM- $\Sigma\Delta$ closed-loop interfaces for an accelerometer or gyroscope chip would be interesting future work.

VII. CONCLUSION

As can be seen from this review, there are a number of well-established advantages of EM- $\Sigma\Delta$ force feedback interfaces for MEMS inertial sensors, in particular for high-end applications. Various micro-accelerometers and gyroscopes with different EM- $\Sigma\Delta$ force feedback control architectures have been discussed in detail. Although advanced CMOS process alleviated some drawbacks of closed loop control such as increased power consuming and chip size, other challenges in system complexity, cost and implementation still makes it suitable mainly for inertial navigation and other high performance applications.

A general introduction to second and high-order EM- $\Sigma\Delta$ force feedback control principles has been provided in this paper. Developments in EM- $\Sigma\Delta$ closed-loop MEMS accelerometers and gyroscopes over the last decades have been reviewed. Moreover, a comparison of the EM- $\Sigma\Delta$ control solutions for improving bias instability, noise floor, DR range and FS range has been presented. Also, future development trends and current challenges of EM- $\Sigma\Delta$ force feedback interfaces have been discussed. EM- $\Sigma\Delta$ force feedback control technology currently is the best choice for MEMS accelerometers aiming at navigation-grade applications and competing with traditional macroscopic electro-mechanical accelerometers. As for MEMS vibratory gyroscopes, EM- $\Sigma\Delta$ force rebalance feedback techniques are a good solution for increasing the bandwidth, linearity, DR and FS range; and alleviating performance degradations due to microfabrication tolerances. In general, the design and development of EM- $\Sigma\Delta$ inertial sensors should take into account multi-physics aspects including the mechanical sensing element, control theory, $\Sigma\Delta$ architectures and system parameter optimization. As the ease of designing and implementing EM- $\Sigma\Delta$ interface circuits continues to mature, researchers will increasingly turn towards it as tools for designing high performance MEMS inertial sensors.

ACKNOWLEDGMENT

The authors wish to thank Dr. Yunfeng Dong, Dr. Bader Almutairi and Dr. Reuben Wilcock for their useful input, and

also thank Prof. Weizheng Yuan and Prof. Honglong Chang for their support during the last years.

REFERENCES

- [1] N. Yazdi, F. Ayazi, K. Najafi, Micromachined inertial sensors, *Proc. IEEE*, vol.86, pp.1640-1659, 1998.
- [2] L. Robin, E. Mounier, Inertial sensor market moves to combo sensors and sensor hubs, 2013. Available: http://www.yole.fr/iso_upload/Mag/Analyst%20corner.pdf
- [3] M. Perlmutter and L. Robin, High-performance, low cost inertial MEMS: A market in motion!, *IEEE/ION Position Location and Navigation Symposium (PLANS)*, 2012, pp.225-229.
- [4] R. Bogue, Recent developments in MEMS sensors: A review of applications, markets and technologies, *Sensor Review*, vol.33, pp.300-304, 2013.
- [5] M. Tanenhaus, D. Carhoun, T. Geis, E. Wan, and A. Holland, Miniature IMU/INS with optimally fused low drift MEMS gyro and accelerometers for applications in GPS-denied environments, *IEEE/ION Position Location and Navigation Symposium (PLANS)*, 2012, pp.256-264.
- [6] M. Lapinski, M. Feldmeier, J.A. Paradiso, wearable wireless sensing for sports and ubiquitous interactivity, *IEEE Conf. Sensors*, Limerick, Ireland, 2011, pp. 1425-1428.
- [7] H. Xie, G. Feder, Integrated microelectromechanical gyroscopes, *J. Aerosp. Eng.*, vol.16, pp. 65-75, 2003.
- [8] S. Beeby, G. Ensell, M. Kraft, N. White, *MEMS mechanical sensors*, Artech House Inc, 2004.
- [9] B. Borovic, A.Q. Liu, D. Popa, H. Cai, F.L. Lewis, Open-loop versus closed-loop control of MEMS devices: choices and issues, *J. Microelectromech. Microeng.*, vol.15, pp. 1917-1924, 2005.
- [10] E. Gaura, R. Newman, M. Kraft, *Smart MEMS and sensor systems*, London: Imperial College Press, 2006.
- [11] J. Soen, A. Voda, C. Cyril, Controller design for a closed-loop micromachined accelerometer, *Control Engineering Practice*, vol.15, pp. 57-68, 2007.
- [12] M. Kraft, R. Wilcock, B. Almutairi, Innovative control systems for MEMS inertial sensors, *IEEE International Frequency Control Symposium (FCS)*, 2012, pp.1-6.
- [13] J.I. Seeger, X. Jiang, M. Kraft and B.E. Boser, Parallel-plate driven oscillations and resonant pull-in, in *IEEE Solid-state sensor, actuator and Microsystems workshop*, Hilton Head, USA, 2002, pp.313-316.
- [14] A. Fargas-Marques, J. Casals-Terre, A.M. Shkel, Resonant pull-in condition in parallel-plate electrostatic actuators, *J. Microelectromech. Syst.*, vol.16, pp. 1044-1053, 2007.
- [15] M. Kraft, C.P. Lewis, T.G. Heskeith, Closed-loop silicon accelerometers, *IEEE Proceedings-Circuits, Devices and Systems*, vol.145, pp. 325-331, 2002.
- [16] M.A. Lemkin, M.A. Ortiz, N. Wongkomet, B.E. Boser, and J.H. Smith, A 3 axis surface micromachined sigma delta accelerometer, *IEEE Solid-State Circuits Conference*, San Francisco, USA, 1997, pp.202-203.
- [17] X. Jiang, J.I. Seeger, M. Kraft and B.E. Boser, A monolithic surface micromachined Z axis gyroscope with digital output, in *Proc. Symp. VLSI Circuits*, Honolulu, 2000, pp.16-19.
- [18] H. Inose, Y. Yasuda and J. Murakami, A telemetering system by code modulation- $\Delta\Sigma$ modulation, *IRE Trans. Space Electronics and Telemetry*, vol.8, pp.204-209, 1962.
- [19] R.J.V.de Plassche, A sigma-delta modulators as an A/D converter, *IEEE Trans. Circuits and Systems*, vol.25, pp.510-514, 1978.
- [20] X. Jiang, Capacitive position-sensing interface for micromachined inertial sensors, *Ph.D. dissertation*, University of California, Berkeley, 2003.
- [21] P. Aziz, H. Sorensen and J. van der Spiegel, An overview of sigma-delta converters, *IEEE Signal Processing Magazine*, vol.13, pp.61-84, 1996.
- [22] H. Kulah, J. Chae and K. Najafi, Noise analysis and characterization of a sigma-delta capacitive silicon microaccelerometer, *12th Conf. on Solid-State Sensors, Actuators and Microsystems (Transducers '03)*, Boston, USA, 2003, pp. 95-98.
- [23] V.P. Petkov and B.E. Boser, A fourth-order $\Sigma\Delta$ interface for micromachined inertial sensors, *IEEE J. Solid-State Circuits*, vol.40, pp.1602-1609, 2005.
- [24] V.P. Petkov, B.E. Boser, High-order electromechanical $\Sigma\Delta$ modulation in micromachined inertial sensors, *IEEE Trans. Circuits Systems I: Regular Papers*, vol.53, pp. 1016-1022, 2006.
- [25] Y. Dong, Control Systems for Capacitive Micromachined Inertial Sensors with high-order sigma-delta modulators, *Ph.D. dissertation*, University of Southampton, 2006.
- [26] T. Smith et al., A 15b electromechanical sigma-delta converter for acceleration measurements, *IEEE Solid-State Circuits Conference*, San Francisco, USA, 1994, pp.160-161.
- [27] J. Raman, P. Rombouts, L. Weyten, An Unconstrained architecture for systematic design of higher order $\Sigma\Delta$ force-feedback loops, *IEEE Trans. Circuits Systems I: Regular Papers*, vol.55, pp. 1601-1614, 2008.
- [28] C.D. Ezekwe, B.E. Boser, Robust compensation of a force-balanced high-Q gyroscope, *IEEE Conf. Sensors*, Lecce, Italy, 2008, pp. 795-798.
- [29] C.D. Ezekwe, B.E. Boser, A mode-matching $\Delta\Sigma$ closed-loop vibratory-gyroscope readout interface with a 0.004 %/√Hz noise floor over a 50Hz band, *IEEE J. Solid-State Circuits*, vol.43, pp.3039-3048, 2008.
- [30] G. Bourdopoulos, A. Pnevmatikakis, V. Anastassopoulos, T. Deliyannis, *Delta Sigma modulator: Modeling, design, and applications*, London: Imperial College Press, 2003.
- [31] L. Breems and J.H. Huijsing, *Continuous-Time Sigma-Delta Modulation for A/D Conversion in Radio Receivers*, Kluwer Academic Publisher, 2001.
- [32] L. Breems, R. Rutten, and G. Wetzker, A cascaded continuous-time $\Sigma\Delta$ Modulator with 67dB dynamic range in 10MHz bandwidth, *IEEE J. Solid-State Circuits*, vol.39, pp.2152-2160, 2004.
- [33] S. Brigati, F. Francesconi, P. Malcovati and F. Maloberti, A fourth-order single-bit switched-capacitor $\Sigma\Delta$ modulator for distributed sensor applications, *IEEE Trans. Instrum. Measurement*, vol.53, pp. 266-270, 2004.
- [34] Z.M. Lin and W.H. Sheu, A generic multiple-feedback architecture and method for the design of high-order $\Sigma\Delta$ modulators, *IEEE Trans. Circuits Systems II: Analog Digital Signal Process.* vol.49, pp.465-473, 2002.
- [35] B. Almutairi, Multi stage noise shaping (MASH) sigma delta modulator for capacitive MEMS Inertial Sensors, *Ph.D. dissertation*, University of California, Berkeley, 2014.
- [36] R. Schreier, G.C. Temes, *Understanding delta-sigma data converters*, New Jersey: John Wiley & Sons, Inc, 2005.
- [37] B. Almutairi, M. Kraft, Multi stage noise shaping sigma-delta modulator (MASH) for capacitive MEMS accelerometers, *Sensors Actuators A*, vol.186, pp.169-177, 2012.
- [38] W. Henrion, L. DiSanza, M. Lp, S. Terry, H. Jarman, Wide dynamic range direct digital accelerometer, *IEEE Solid-State Sensor and Actuator Workshop*, San Francisco, USA, 1990, pp.153-157.
- [39] W. Yun, R.T. Howe and P.R. Gray, Surface micromachined, digitally force-balanced accelerometer with integrated CMOS detection circuitry, *IEEE Solid-State Sensor and Actuator Workshop*, San Francisco, USA, 1992, pp.126-131.
- [40] C. Lu, M. Lemkin and B. Boser, A monolithic surface micromachined accelerometer with digital output, *IEEE Solid-State Circuits Conference*, San Francisco, USA, 1995, pp.160-161.
- [41] B. Boser and R. Howe, Surface micromachined accelerometers, *IEEE J. Solid-State Circuits*, vol.31, pp.366-375, 1996.
- [42] M. Lemkin and B. Boser, A three-axis micromachined accelerometer with a CMOS position-sense interface and digital offset-trim electronics, *IEEE J. Solid-State Circuits*, vol.34, pp.456-468, 1999.
- [43] N.Yazdi and K. Najafi, Performance limits of a closed-loop, micro-g silicon accelerometer with deposited rigid electrodes, in *Proc. 12th Int. Conf. MicroElectronics*, Tehran, Iran, 2000, pp. 313-316.
- [44] H. Kulah, J. Chae and K. Najafi, Noise analysis and characterization of a sigma-delta capacitive microaccelerometer, *IEEE J. Solid-State Circuits*, vol.41, pp.352-361, 2006.
- [45] J. Wu, Sensing and control electronics for low-mass low-capacitance MEMS accelerometers, *Ph.D. dissertation*, Carnegie Mellon University, 2002.
- [46] T. Kajita, U.K. Moon and G.C. Temes, A two-chip interface for a MEMS accelerometer, *IEEE Trans. Instrum. Measurement*, vol.51, pp. 853-858, 2002.
- [47] B.V. Amini, R. Abdolvand and F. Ayazi, A 4.5-mW closed-loop $\Delta\Sigma$ micro-gravity CMOS SOI accelerometer, *IEEE J. Solid-State Circuits*, vol.41, pp.2983-2991, 2006.

- [48] B.V. Amini, S. Pourkamali and F. Ayazi, A 2.5V 14-bit $\Sigma\Delta$ CMOS-SOI capacitive accelerometer, *IEEE Solid-State Circuits Conference*, 2004, pp.314-530.
- [49] Y. Dong, M. Kraft, C. Gollasch, W. Redman-white, A high-performance accelerometer with a fifth-order sigma-delta modulator, *J. Micromech. Microeng.* vol.15, pp. 1-8. 2005.
- [50] I. Sari, I. Zeimpekis, M. Kraft, A dicing free SOI process for MEMS devices, *Microelectron. Eng.*, vol.95, pp. 121-129. 2012.
- [51] Y. Dong, M. Kraft, and W. Redman-white, Force feedback linearization for higher-order electromechanical sigma-delta modulators, *J. Micromech. Microeng.* vol.16, pp. 54-60. 2006.
- [52] F. Chen, W. Yuan, H. Chang, I. Zeimpekis, M. Kraft, low noise vacuum MEMS closed-loop accelerometer using sixth-order multi-feedback loops and local resonator sigma delta modulator, *27th IEEE Int. Conf. Micro Electro Mech. Syst.*, San Francisco, USA, 2014, pp.761-764.
- [53] U. Sonmez, H. Kulah, T. Akin, A fourth order unconstrained $\Sigma\Delta$ capacitive accelerometer, *16th Conf. on Solid-State Sensors, Actuators and Microsystems (Transducers'11)*, Beijing, China, 2011, pp. 707-710.
- [54] M. Pastre et al., A 300Hz 19b DR capacitive accelerometer based on a versatile front end in a 5th-order delta-sigma loop, *35th European Solid-State Circuits Conference*, Athens, Greece, 2009, pp.299-291.
- [55] M. Pastre et al., A navigation-grade MEMS accelerometer based on a versatile front end, *37th Annual conference on IEEE Industrial Electronics Society*, 2011, pp.4038-4043.
- [56] Y. Dong et al., High performance inertial navigation grade sigma-delta MEMS accelerometer, *IEEE/ION position location and navigation symposium (PLANS)*, 2010, pp.32-36.
- [57] P. Zwahlen et al., Navigation grade MEMS accelerometer, *23rd IEEE Int. Conf. Micro Electro Mech. Syst.*, Hong Kong, 2010, pp.631-634.
- [58] Y. Dong et al., Ultra-high precision MEMS accelerometer, *16th Conf. on Solid-State Sensors, Actuators and Microsystems (Transducers'11)*, Beijing, China, 2011, pp. 695-696.
- [59] P. Zwahlen et al., Breakthrough in high performance inertial navigation grade sigma-delta MEMS accelerometer, *IEEE/ION position location and navigation symposium (PLANS)*, 2012, pp.15-19.
- [60] Honeywell, Datasheet QA2000 Q-Flex® Accelerometer: The inertial navigation standard, Available: <http://www.inertialsensor.com/docs/qa2000.pdf>.
- [61] J. Wu and L.R. Carley, Electromechanical $\Delta\Sigma$ modulation with high-Q micromechanical accelerometers and pulse density modulated force feedback, *IEEE Trans. Circuits Systems I: Regular Papers*, vol.53, pp. 274-287, 2006.
- [62] H. Xu, X. Liu and L. Yin, A closed-loop $\Sigma\Delta$ interface for a high-Q micromechanical capacitive accelerometer with 200ng/ $\sqrt{\text{Hz}}$ input noise density, *IEEE J. Solid-State Circuits*, vol.50, pp.2101-2112, 2015.
- [63] G. Krishnan et al., Micromachined high-resolution accelerometers, *J. Indian Institute of Science*, vol. 87:3, pp.333-361, 2007
- [64] B. Almutairi, M. Kraft, Experimental study of single loop sigma-delta and multi stage noise shaping (MASH) modulators for MEMS accelerometer, *IEEE Conf. Sensors*, Limerick, Ireland, 2011, pp. 520-523.
- [65] B. Almutairi, M. Kraft, Comparative study of multi stage noise shaping and single loop sigma delta modulators for MEMS accelerometers, *Proc. Eurosensors XXIV*, vol.5, pp. 512-515, 2010.
- [66] B. Almutairi, M. Kraft, Multi stage noise shaping sigma-delta modulator (MASH) for capacitive MEMS accelerometers, *Eurosensors XXV*, vol.25, pp.1313-1316, 2011.
- [67] B. Almutairi, A. Alshehri, M. Kraft, MASH2-0 electromechanical sigma-delta modulator for capacitive MEMS sensors using dual quantization method, *IEEE Conf. Sensors*, Valencia, Spain, 2014, pp. 1780-1783.
- [68] B. Almutairi, A. Alshehri, M. Kraft, Design and implementation of a MASH2-0 electromechanical sigma-delta modulator for capacitive MEMS sensors using dual quantization method, *J. Microelectromech. Syst.*, vol.24, pp. 1251-1263, 2015.
- [69] J. Cui, X. Z. Chi, H. T. Ding, L. T. Lin, Z. C. Yang, G. Z. Yan, Transient response and stability of the AGC-PI closed-loop controlled MEMS vibratory gyroscopes, *J. Micromech. Microeng.* vol.19, pp. 1-17. 2009.
- [70] R. Oboe, R. Antonello, E. Lasalandra, G. S. Durante, L. Prandi, Control of a Z-axis MEMS vibrational gyroscope, *IEEE/ASME Trans. Mechatron.*, vol.10, pp. 364-370, 2005.
- [71] R. T. M'Closkey and A. Vakakis, Analysis of a microsensor automatic gain control loop, in *proc. American Control Conf.*, San Diego, USA, 1999, pp. 3307-3311.
- [72] Y. C. Chen, R. T. M'Closkey, T. A. Tran, B. Blaes, A control and signal processing integrated circuit for the JPL-Boeing micromachined gyroscopes, *IEEE trans. Control Syst. Technol.*, vol.13, pp.286-300, 2005.
- [73] D. J. Kim, R. T. M'Closkey, Real-time tuning of JPL-Boeing MEMS gyro dynamics, *American control conf.*, Portland, USA, 2005, pp.3598-3603.
- [74] W. T. Sung, S. Sung, J. Y. Lee, T. Kang, Y. J. Lee and J. G. Lee, Development of a lateral velocity-controlled MEMS vibratory gyroscope and its performance test, *J. Micromech. Microeng.* vol.18, pp. 1-17. 2008.
- [75] X. Jiang, J.I. Seeger, M. Kraft and B.E. Boser, A monolithic surface micromachined z-axis gyroscope with digital output, *Symposium on VLSI Circuits*, Honolulu, USA, 2000, PP. 16-19.
- [76] H. Rodjegard, D. Sandstrom, P. Pelin, N. Hedenstierna, D. Eckerbert, G. I. Andersson, A digitally controlled MEMS gyroscope with 3.2 deg/Hr stability, *13th Conf. on Solid-State Sensors, Actuators and Microsystems (Transducers'05)*, Seoul, Korea, 2005, pp. 535-538.
- [77] N. Hedenstierna, S. Habibi, S.M. Nilsen, T. Kvisteroy, G.U. Jensen, Bulk micromachined angular rate sensor based on the butterfly-gyro structure, *14th IEEE Int. Conf. Micro Electro Mech. Syst.*, Interlaken, Switzerland, 2001, pp.178-181.
- [78] J. Raman, E. Cretu, P. Rombouts, L. Weyten, A closed-loop digitally controlled MEMS gyroscope with unconstrained sigma-delta force-feedback, *IEEE J. Sensors*, vol.9, pp. 297-305, 2009.
- [79] J. Raman, E. Cretu, P. Rombouts, L. Weyten, A digitally controlled MEMS gyroscope with unconstrained sigma-delta force-feedback architecture, in *Proc. 19th IEEE Int. Conf. Micro Electro Mech. Syst.*, Istanbul, Turkey, 2006, pp. 710-713.
- [80] S. Rombach, T. Northemann, M. Maurer, M. Dienger, Y. Manoli, Modulated electromechanical continuous-time low pass sigma delta modulator for micromachined gyroscopes, *16th Conf. on Solid-State Sensors, Actuators and Microsystems (Transducers'11)*, Beijing, China, 2011, pp. 1092-1095.
- [81] A. Elsayed et al. A self-clocked ASIC interface for MEMS gyroscope with 1m %s / $\sqrt{\text{Hz}}$ noise floor, *IEEE Custom Integrated Circuits Conference*, San Jose, USA, 2011, PP.1-4.
- [82] SWS configurable inertial sensing ASIC and development platform, Available: <http://www.si-ware.com/asic-solutions/>
- [83] A. Sharma, M. F. Zaman, F. Ayazi, A sub-0.2 %hr bias drift micromechanical silicon gyroscope with automatic CMOS mode-matching, *IEEE J. Solid-State Circuits*, vol.44, pp.1593-1608, 2009.
- [84] Y. Dong, M. Kraft, W. Redman-White, High order band-pass sigma delta interfaces for vibratory gyroscopes, in *Proc. 4th IEEE Conf. Sensors*, Irvine, USA, 2005, pp. 1080-1083.
- [85] C.D. Ezekwe, B.E. Boser, A mode-matching $\Delta\Sigma$ closed-loop vibratory gyroscope readout interface with a 0.004 %s / $\sqrt{\text{Hz}}$ noise floor over a 50Hz band, *IEEE Solid-State Circuits Conference*, San Francisco, USA, 2008, pp.580-637.
- [86] T. Northemann, M. Maurer, S. Rombach, A. Buhmann, Y. Manoli, A digital interface for gyroscopes controlling the primary and secondary mode using band-pass sigma-delta modulation, *Sensors Actuators A*, vol.162, pp.388-393, 2009.
- [87] T. Northemann, M. Maurer, A. Buhmann, L. He, Y. Manoli, Excess loop delay compensated electro-mechanical bandpass sigma-delta modulator for gyroscopes, *Proc. Eurosensors XXIII Conference*, 2009, pp.1183-1186.
- [88] T. Northemann, M. Maurer, S. Rombach, A. Buhmann, Y. Manoli, Drive and sense interface for gyroscopes based on bandpass sigma-delta modulators, *Proc. IEEE Int. Symposium on Circuits and Systems*, Paris, France, 2010, pp.3264-3267.
- [89] Y. Dong, M. Kraft, W. Redman-White, Micromachined Vibratory gyroscopes controlled by a high-order band-pass sigma-delta modulator, *IEEE J. sensors*, vol.7, pp. 59-69, 2007.
- [90] Y. Dong, M. Kraft, W. Redman-White, High order noise shaping filters for high performance inertial sensors, *IEEE Trans. Instrum. Measurement*, vol.56, pp. 1666-1674, 2007.
- [91] Y. Dong, M. Kraft, N. Hedenstierna, W. Redman-White, Microgyroscope Control system using a high-order band-pass continuous-time sigma-delta modulator, *Sensors Actuators A*, vol. 145-146, pp.299-305, 2008.

- [92] J.A. Cherry, W.M. Snelgrove, Excess loop delay in continuous-time delta-sigma modulators, *IEEE Trans. Circuits Systems II: Analog Digital Signal Process.* vol.46, pp.376-389, 1999.
- [93] S. Nessler, M. Marx, M. Maurer, S. Rombach, Y. Manoli, A continuous-time collected force-feedback and readout front end for MEMS gyroscopes, *41st European Solid-State Circuits Conference, Graz, 2015*, pp.408-411.
- [94] A. Ismail et al., A high performance MEMS based digital-output gyroscope, *17th Conf. on Solid-State Sensors, Actuators and Microsystems (Transducers '13)*, Barcelona, Spain, 2013, pp. 2523-2526.
- [95] S.H. Ardalan, J.J. Paulos, An analysis of nonlinear behavior in Delta-Sigma modulators, *IEEE Trans. Circuits Syst.-I*, vol.34, pp.593-603, 1987.
- [96] M. Lemkin, Micro accelerometer design with digital feedback control, *Ph.D. thesis*, University of California Berkeley, 2003.
- [97] J. Lota, M. Al-Janabi, I. Kale, Nonlinear-stability analysis of higher order $\Delta-\Sigma$ modulators for DC and sinusoidal inputs, *IEEE Trans. Instrum. Meas.*, vol.57, pp.530-542, 2008.
- [98] R. Wilcock, M. Kraft, Genetic algorithm for the design of electro-mechanical Sigma Delta Modulator MEMS Sensors, *MDPI J. Sensors*, vol.10, pp.9217-9238, 2011.
- [99] F. Chen, H.L. Chang, W.Z. Yuan, R. Wilcock, M. Kraft, Parameter optimization for a high-order band-pass continuous-time sigma-delta modulator MEMS gyroscope using a genetic algorithm approach, *J. Micromech. Microeng.* vol.22 (105006), 2012.
- [100] F. Chen, W.Z. Yuan, H.L. Chang, G.M. Yuan, J.B. Xie, M. Kraft, Design and Implementation of an optimized double closed-loop control system for MEMS vibratory gyroscope, *IEEE Sensors J.*, vol.14, pp.184-196, 2014.
- [101] Colibrys MEMS accelerometers, Available: <http://www.colibrys.com/c/technology/mems-accelerometers/>
- [102] Imego AB high-end MEMS gyroscope and accelerometer solutions, Available: <http://www.imego.com/>



Fang Chen received the B.S., M.S., and Ph.D. degrees in mechanical and electronic engineering from Northwestern Polytechnical University (NPU), Xi'an, China. He is currently a Research Staff Member with the Shanghai Institute of Microsystem and Information Technology, Chinese Academy of Sciences, Shanghai, China. From 2010 to 2011, he was a visiting

Ph.D. student with the Nano Group, School of Electronics and Computer Science, University of Southampton, UK. His current research interests include MEMS inertial sensors, EM- $\Sigma\Delta$ force feedback closed-loop circuits.



Xinxin Li received the B.S. degree in Semiconductor physics and devices from Tsinghua University, Beijing, China, in 1987, and the Ph.D. degree in microelectronics from Fudan University, Shanghai, China, in 1998. For a long period time, his research interests have been in the fields of micro/nano sensors and MEMS/NEMS.

He was a research engineer with Shenyang Institute of Instrumentation Technology, Shenyang, China, for five years. He was also with Hong Kong University of Science and Technology, Kowloon, Hong Kong, as a Research Associate and with Nanyang Technological

University, Singapore, as a Research Fellow. He then joined Tohoku University, Sendai, Japan, as a Lecturer (Center of Excellence Research Fellowship). Since 2001, he has been a professor with the Shanghai Institute of Microsystem and Information Technology, Chinese Academy of Sciences, Shanghai. From 2007 he has been serving as the Director of the State Key Laboratory of Transducer Technology, China. He has invented more than 80 patents and published more than 300 papers in refereed journals and conference proceedings (including about 160 SCI papers). He is on the Editorial Board of the Journal of Micromechanics and Microengineering. Prof. Xinxin Li served as the technical Program Committee member for IEEE MEMS 2008 and 2011, IEEE Sensors from 2002 to 2014. From 2014, he has been serving as an International Steering Committee member for the conference on Solid-State Sensors, Actuators and Microsystems (Transducers).



Michael Kraft received a Dipl.-Ing.(Univ.) degree in electrical and electronics engineering from the Friedrich Alexander Universität Erlangen-Nürnberg, Germany, in 1993 and a Ph.D. degree from Coventry University, Coventry, U.K., in 1997. He is currently a professor of Micro- and Nano-systems with the University of Liege, Belgium, and a Guest Professor

with Shanghai Institute of Microsystem and Information Technology, Chinese Academy of Sciences. Before joining the University of Liege, from 2012 to 2014 he was with the Fraunhofer Institute for Microelectronic Circuits and Systems, Duisburg, Germany, heading the department of Micro- and Nano-systems with a focus on fully integrated microsensors and biohybrid systems. Concurrently, he held the professorial Chair (W3) of Integrated Micro- and Nano-systems with the University of Duisburg-Essen. From 1999 to 2012, he was an academic at the School of Electronics and Computer Science, University of Southampton, Southampton, U.K, where he also acted as the Director of the Southampton Nanofabrication Centre from 2010-2012. He also spent two years at the Berkeley Sensors and Actuator Centre, University of California, Berkeley, working on integrated MEMS gyroscopes. In his career he has focused on novel micro- and nanofabrication techniques, microsensors, and actuators and their interface circuits, particularly for capacitive sensors. He has a broad interest in MEMS and nanotechnology ranging from process development to system integration of MEMS and nanodevices. He has published over 200 peer-reviewed journal and conference papers as an author or coauthor. He also contributed to three text books on MEMS and edited a book on MEMS for aerospace and automotive applications.

Dr. Kraft has served on several steering and technical committees of international conferences such as IEEE Sensors, Eurosensors, and the Micromechanics and Microsystems Europe Workshop.